UNIVERSITAT POLITÈCNICA DE VALÈNCIA

School of Telecommunications Engineering

Experimental characterization of optical frequency combs in silicon nitride ring resonators

End of Degree Project

Bachelor's degree in Engineering Physics

AUTHOR: Ros Bisbal, Alba

Tutor: Martínez Abietar, Alejandro José

Cotutor: Mercadé Morales, Laura

Cotutor: Milián Enrique, Carles

Experimental director: Molina Grífols, Pol

ACADEMIC YEAR: 2024/2025

Resumen

Este proyecto fin de carrera presenta el estudio experimental de un circuito fotónico integrado de nitruro de silicio (Si_3N_4), diseñado para investigar el comportamiento óptico de micro anillos resonantes, con especial atención a fenómenos no lineales como el efecto termo-óptico y la formación de solitones de Kerr disipativos. El trabajo incluye una descripción de los montajes horizontales experimentales utilizados para las medidas tanto en transmisión como en reflexión, seguida del procedimiento de alineación y el análisis de los espectros de resonancia. El objetivo principal de este proyecto es la observación y caracterización de peines de frecuencia ópticos; sin embargo, no pudimos alcanzar el régimen de formación de solitones debido a algunas dificultades de configuración. No obstante, los resultados proporcionan una valiosa visión del comportamiento de los anillos resonantes integrados bajo altas potencias ópticas y sientan las bases para futuras mejoras en la estabilidad experimental y la generación de solitones.

Resum

Este projecte de fi de carrera presenta l'estudi experimental d'un circuit fotònic integrat de nitrur de silici (Si_3N_4), dissenyat per a investigar el comportament òptic de micro anells ressonants, amb especial atenció a fenòmens no lineals com l'efecte termo-òptic i la formació de solitons de Kerr dissipatius. El treball inclou una descripció dels muntatges horitzontals experimentals utilitzats per a les mesures tant en transmissió com en reflexió, seguida del procediment d'alineació i l'anàlisi dels espectres de ressonància. L'objectiu principal d'este projecte és l'observació i caracterització de pintes de freqüència òptics; no obstant això, no vam poder aconseguir el règim de formació de solitons a causa d'algunes dificultats de configuració. No obstant això, els resultats proporcionen una valuosa visió del comportament dels anells ressonants integrats sota altes potències òptiques i establixen les bases per a futures millores en l'estabilitat experimental i la generació de solitons.

Abstract

This final degree project presents the experimental study of a silicon nitride (Si_3N_4) photonic integrated circuit, designed to investigate the optical behavior of microring resonators, with special focus on nonlinear phenomena such as the thermo-optic effect and the formation of dissipative Kerr solitons. The work includes a description of the horizontal experimental setups used for both transmission and reflection measurements, followed by the alignment procedure and the analysis of resonances spectra. The main goal of this project is the observation and characterization of optical frequency combs; however, we were not able to reach the soliton formation regime due to some setup difficulties. Nevertheless, the results provide valuable insight into the behavior of integrated ring resonators under high optical powers and lay the groundwork for future improvements in experimental stability and soliton generation.

UNIVERSITAT POLITÈCNICA DE VALÈNCIA

TELECOM ESCUELA TÉCNICA VLC SUPERIOR DE INGENIERÍA DE TELECOMUNICACIÓN

EXECUTIVE SUMMARY

The Bachelor's / Master's thesis must develop in the text the following concepts, appropriately justified and discussed, focusing on the field of FIELD OF STUDY

CONCEPT (ABET)	Done? (Y/N)	Where? (page numbers)
1. IDENTIFY:		
1.1. Problem statement and opportunity	Yes	1-5
1.2. Constraints (standards, codes, needs, requirements & specifications)	Yes	1-3, 12-19
1.3. Setting of goals	Yes	4
2. FORMULATE:		
2.1. Creative solution generation (analysis)	Yes	12-19, 22-25
2.2. Evaluation of multiple solutions and decision-making (synthesis)	Yes	19-30
3. SOLVE:		
3.1. Fulfilment of goals	Yes	31
3.2. Overall impact and significance (contributions and practical recommendations)	Yes	31

Table of contents

Chapter 1. INTRODUCTION

The integration of photonic components on a single chip has revolutionized the field of optics, enabling scalable, compact and efficient systems for many different applications. This project focuses on the experimental study of microring resonators implemented in a Si_3N_4 photonic integrated circuit (PIC), with the purpose of studying their linear and nonlinear optical behavior, including the potential observation of temporal solitons and the frequency comb generation.

1.1 State of the art and motivation

Photonic integrated circuits (PICs) have become a key technology in the development of modern optical systems, enabling compact, scalable and low-loss devices for applications in telecommunications, sensing, signal processing and quantum information. By integrating multiple optical components on a single chip, PICs offer better characteristics than what electronic integrated circuits achieved in the last century. Among the various platforms available, Silicon Nitride (Si_3N_4) stands out due to its ultra-low propagation losses, wide transparency window, and compatibility with CMOS fabrication processes. Recent reviews highlight its progress in integration, including high-Q resonators and electrically pumped frequency comb sources [1].

Within this field, microring resonators stand out because of their compact size and strong light confinement. These structures form the basis for nonlinear optical experiments, as they can support the generation of Kerr solitons and optical frequency combs, which have been demonstrated in Si_3N_4 microresonators with high Q factors. Optical frequency combs have fundamentally transformed metrology, spectroscopy, timekeeping, and a range of other applications, such as frequency metrology, LIDAR and optical clocks … (*Figure 1*) [1].

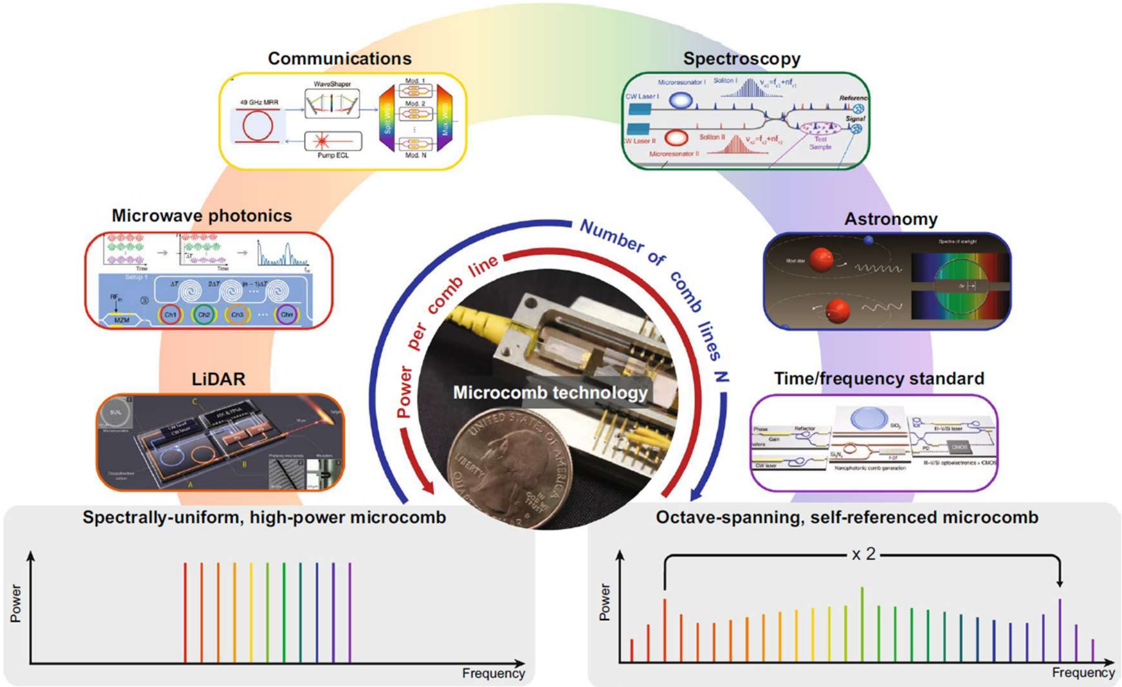

Figure 1. Application-driven development of microcombs. The arrows around the microcomb module indicate the relative importance of the power and number of comb lines for different applications, which include microwave photonics, LiDAR, communications, spectroscopy, astronomical calibration, and time/frequency standard (Figure obtained from Ref. [1])

Despite these achievements, generating and stabilizing solitons in integrated resonators remains challenging. It requires precise control of resonance and coupling conditions, power levels, dispersion and polarization, as well as an understanding of the physical mechanisms such as the Kerr and thermo-optic effects.

Optical frequency comb-based technologies in the past years were mainly deployed in research laboratories because they usually depended on bulky, power-hungry, expensive equipment to generate, control and manipulate the comb light. Over the past twenty years, the blooming of integrated photonics has allowed the production of devices for frequency comb formation using advanced lithography and nanofabrication techniques, which offer great advantages in lowering the system size, weight and power consumption, and cost. Therefore, it holds the potential to accelerate the transition from research laboratory experiments to consumer applications [2]. In *Figure 2*, there is a timeline with the evolution of these technologies.

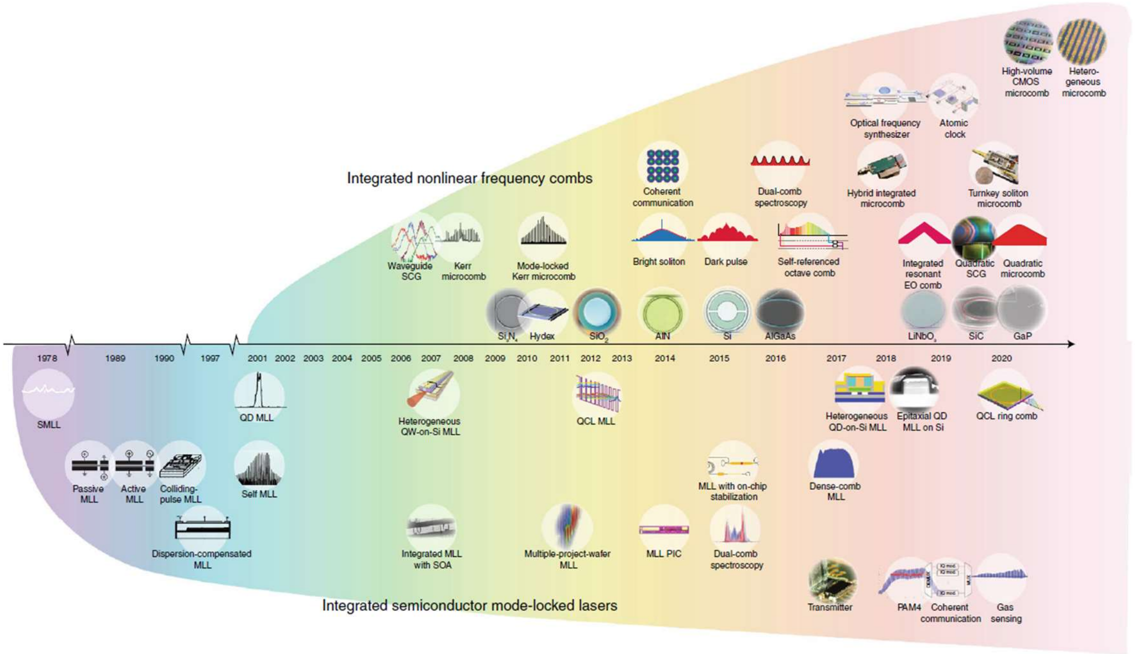

Figure 2. Timeline of the evolution of optical frequency comb technologies (Figure extracted from Ref. [2])

This project is motivated by the opportunity to contribute to this line of research through the experimental characterization and alignment of a Si_3N_4 PIC containing microring resonators. By studying the resonance behavior under different input conditions and attempting to reach the soliton formation, this work aims to deepen the understanding of nonlinear effects in integrated photonics and explore the necessary conditions for comb generation in experimental setups.

1.2 Methodology and chronogram

This experimental project was carried out over five months, from March to July. It began with a literature review to understand the key concepts related to microring resonators and photonic integrated circuits (PICs), the effects that can occur in these structures and some measurement techniques. In the meantime, we started the experimental characterization and optimized the two experimental setups that include different optical components, which are described in detail in the section dedicated to the experimental setup. In that section, we also describe the sample with the PIC and the process of alignment, which is important to carry out before taking the experimental measurements. In May and June, most of the experimental work was conducted and data was collected either with the power meter, the OSA or with the oscilloscope. The final phase, conducted mostly in July, focused on data analysis with Python and Origin software and writing the thesis. Many figures were made or edited using Inkscape or DigitalMicrograph. A Gantt chart with the project phases and their duration can be found in *Figure 3*.

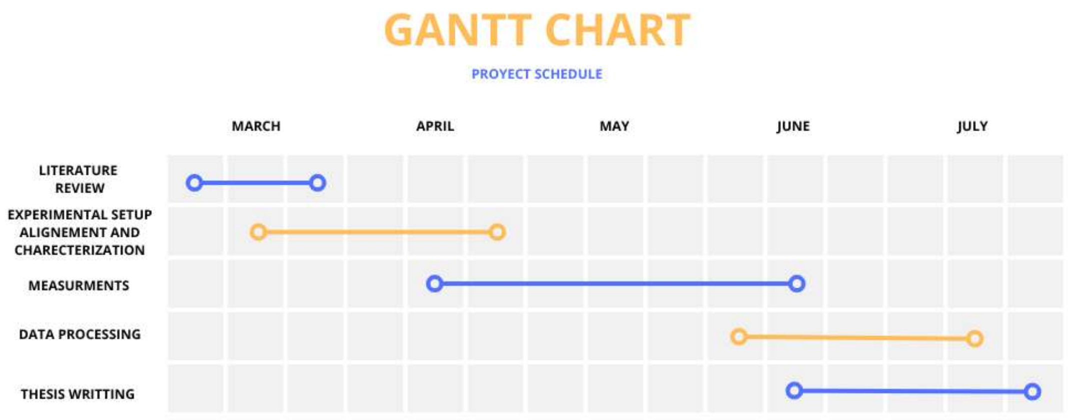

Figure 3. Gantt diagram representation of the work plan

1.3 Objectives

The main goal of this work is the experimental characterization of optical frequency combs in silicon nitride ring resonators. Nevertheless, we divided the experimental work into the following more specific objectives, in chronological order:

- Learn how to use, align and optimize the experimental optical setups.
- Characterization of optical resonances of the ring resonators and calculation of their Q factor.
- Study of the polarization of the rings.
- Ensure that the EDFA is amplifying the signal correctly.
- Observe the thermo-optic effect. This includes seeing steps and irregularities in the resonances and watching the resonances shift as the input power increases.
- Observe optical frequency combs in the OSA at high input powers. This is the final objective as seeing the combs means there has been soliton formation.

These objectives involved practical work in a research laboratory (Nanophotonics Technology Center) and are explained in more detail in the Results section (chapter 4). The experimental setups used for the measurements are also described below in chapter 3 and the theoretical background needed to understand the results in chapter 2.

This project also aligns with the Sustainable Development Goals (SDGs) defined by the United Nations, particularly with Goal 7: Affordable and Clean Energy; and Goal 9: Industry, Innovation and Infrastructure. Integrated photonic systems have the potential to significantly reduce power consumption compared to other traditional methods, such as electric systems, because PIC technologies are more energy-efficient and sustainable. Also, these advanced photonic structures, such as microring resonators, contribute to developing innovative and compact technologies that can be applied in different sectors like telecommunications and sensing [4].

Additionally, this work contributes to Goal 4: Quality Education, as it is part of a university curriculum that allows students to develop practical skills in real laboratory environments and helps them prepare for future careers in high-tech fields such as nanophotonics [4].

Chapter 2. THEORETICAL BACKGROUND

This chapter provides the theoretical foundations necessary to understand the operation of the optical setups and the principles behind the experimental work. It begins with an overview of the key optical components involved, including optical fibers, waveguides and microring resonators, highlighting their roles in guiding and manipulating light. Then there is a section dedicated to the physics of solitons in nonlinear optical resonators, covering how they are formed, the role of Kerr nonlinearities and the generation of optical frequency combs. These concepts together form the basis for understanding the results and phenomena observed throughout the project.

2.1 Optical components

The sample used for the experimental measurements consists of a photonic integrated circuit (PIC) of silicon nitride (Si_3N_4) with two microring resonators coupled to a bus waveguide each. In the section of the experimental characterization there is more information about this chip. The optical components present in the PIC and the optical fibres that guide the light through the setups are described below.

2.1.1 Optical fibres

Optical fibres are cylindrical dielectric waveguides designed to guide light over long or short distances with minimal losses. They are commonly employed in telecommunications, sensing and photonic experiments due to their low attenuation, high bandwidth and immunity to electromagnetic interference [4]. In our setups, fibres are essential for transmitting light from the laser to the PIC and for collecting the signal at the output.

An optical fibre typically consists of a core, where light is guided, surrounded by a cladding with a slightly lower index [4]. Light confinement is ensured by total internal reflection (TIR) at the interface between the core and the cladding, where virtually all the light from the incident ray is reflected. TIR occurs when the incident angle is greater than the critical angle, the obtention of this critical angle can be seen in the following formula:

$$Sin(\theta_C) = \frac{n_{cladding}}{n_{core}}, \tag{2.1}$$

where $n_{core}$and $n_{cladding}$ are the refractive indices of the fibre core and the cladding, respectively [5]. In *Figure 4* there's an image of the light propagation in an optical fibre.

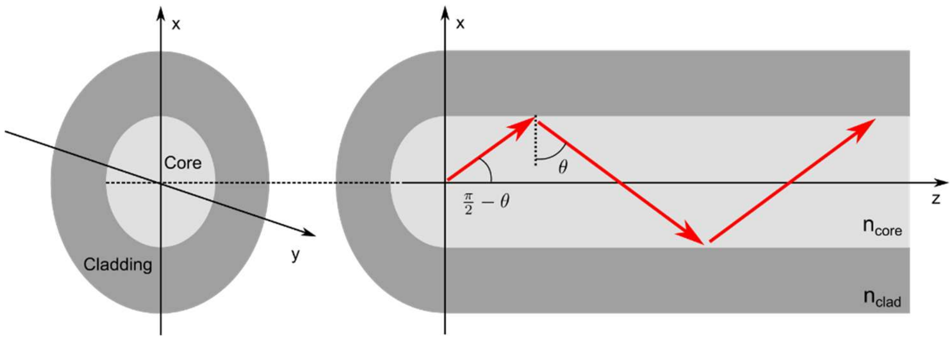

Figure 4. Schematic of opical fiber and a ray confined in the core by TIR (Figure extracted from Ref. [6])

In our experimental setups, light is coupled to the PIC by lensed fibres. These fibres have a tapered or curved end face that focuses the light into a small point, improving coupling efficiency with the waveguides of the chip [6]. Lensed fibres exhibit very low attenuation (~0.2–0.3 dB/km) at 1550 nm (telecom C-band) in short distances as in our work, but in laboratory setups there are important losses that mostly arise from coupling inefficiencies and misalignment [7].

Another important consideration is dispersion and polarization effects. Although chromatic dispersion is usually negligible in short laboratory fibre runs, polarization does impact the experiments. Standard fibres do not preserve polarization which is why polarization-dependent devices like resonators, can show different behavior dependent on the input state of polarization. In many cases, polarization controllers are added before the chip in experimental setups in order to align the polarization with the guided mode of interest, or to optimize the experiments [8].

2.1.2 Waveguide

Integrated optical waveguides are essential components in photonic integrated circuits, enabling the confinement and guiding of light within a planar structure on a chip. Waveguides in photonic chips are typically rectangular and are fabricated using materials of high refractive index, for example, the PIC used in this work is made on silicon nitride [9].

The waveguide consists of a core region surrounded by a cladding with a lower refractive index. As in optical fibres, the light is confined in the core via TIR. This confinement is extremely strong in systems with high index contrast between the core and the cladding, as in Si_3N_4 with SiO_2 [10]. In Table 1 there is a comparison of the properties of various materials suitable for nonlinear photonics.

Material	Refractive index	Nonlinear index ($m^2 W^{-1}$)	Transparency (μm)	KCG observed	SCG observed	$\chi^{(2)}$
Silica	1.45	3×10^{-20}	0.2–4	Y	Y	N
Si	3.47	5×10^{-18}	1.2–8	Y	Y	N
α-Si-H	3.73	1.7×10^{-17}	0.78–4	N	Y	N
Si_3N_4	2.0	2.5×10^{-19}	0.4–4.6	Y	Y	N[c]
Hydex	1.7	1.15×10^{-19}	0.29–7	Y	Y	N
AlN	2.12	2.3×10^{-19}	0.2–13.6	Y	Y	Y
GaN	2.31	7.8×10^{-19}	0.36–13.6	N	N	Y
GaP	3.05	6×10^{-18}	0.54–10.5	Y	N	Y
Diamond	2.38	8×10^{-20}	0.22->50	Y	Y	N
AlGaAs	3.3	2.6×10^{-17}	0.7–17	Y	Y	Y
SiGe[a]	3.59	2.7×10^{-18}	1.2–9.3	N	Y	N
Ge[b]	4.33	4.4×10^{-17}	1.8–15	N	N	N
$LiNbO_3$	2.21	1.8×10^{-19}	0.35–5	Y	Y	Y
As_2S_3	2.43	3.8×10^{-18}	0.6–11	N	Y	N
As_2Se_3	2.81	2.4×10^{-17}	1–14	N	Y	N

Table 1. Linear and nonlinear optical properties of various materials suitable for chip-based nonlinear photonics. Columns 5 and 6 correspond to whether Kerr-comb generation (KCG) and supercontinuum generatiom (SCG), respectively, have been observed. Column 7 indicates whether the material possesses a second-order optical nonlinearity ($\chi^{(2)}$). Y, yes; N, no (Table extracted from Ref. [11])

Propagation of light in waveguides does not follow ray theory, instead it is governed by Maxwell's equations and can be described in terms of guided modes, which are field distributions that satisfy boundary conditions and propagate without changing shape. The wave equation is derived from this Maxwell's equations. The relevant modes in rectangular waveguides are TE (transverse electric) and TM (transverse magnetic) modes, depending on the polarization of the electric field relative to the propagation axis [12].

A key parameter in waveguides is the effective refractive index that characterizes each mode, representing the phase velocity of light within the waveguide. The effective refractive index has a value between the refractive index of the cladding and the refractive index of the core. The phase velocity of the light confined in the waveguide is given by:

$$v_p = \frac{c}{n_{eff}}, \tag{2.2}$$

where c is the speed of light in a vacuum and n_{eff} is the effective index [13].

In summary, integrated waveguides in Si_3N_4 enable compact, low loss light guiding with strong confinement, which is key for efficient coupling and enabling nonlinear effects.

2.1.3 Ring resonators

Microring resonators are integrated optical structures which consist of a close-loop waveguide that is evanescently coupled to one or more straight waveguides. In *Figure 5* there is an optical microscope image of one of the ring resonators coupled to a waveguide, used in the experimental work.

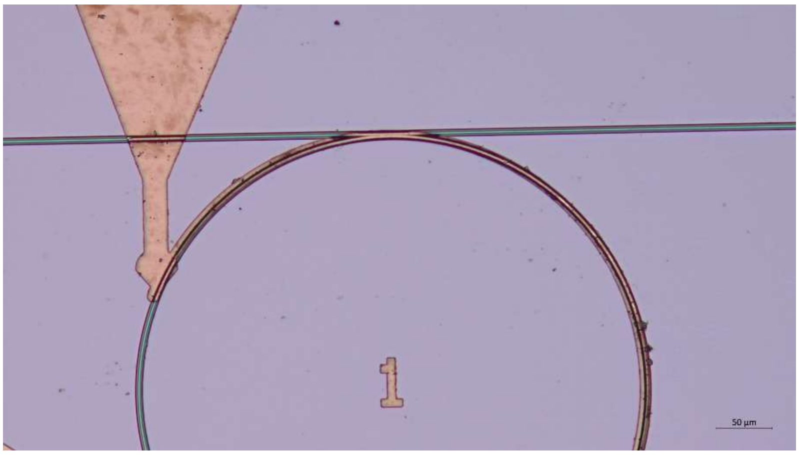

Figure 5. Image of a ring resonator coupled to a waveguide, made with an optical microscope

When the phase condition for resonance is satisfied, light constructively interferes within the ring. A microring resonates when the optical length of the resonator is equal to a multiple of the wavelengths:

$$\lambda_{res} = \frac{n_{eff}L}{m}; m = 1, 2, 3, \ldots$$

(2.3)

where λ_{res} is the resonance wavelength, m is an integer mode number, n_{eff} is the effective index of the guided mode and L is the resonators length which is $L = 2\pi R$ [14].

These devices are fundamental for this project due to their ability to confine light for extended durations, enabling the observation of resonances and soliton formation. They are also quite important in integrated photonics in general, as they are used for filtering, sensing, nonlinear optics…

One of the key parameters when studying ring resonators is the quality factor (Q), defined as:

$$Q = 2\pi \frac{stored\ energy}{disipated\ energy},$$

(2.4)

where the stored and dissipated energy are per cycle and it is a dimensionless parameter. A typically high Q factor for silicon nitride rings is around $10^5 - 10^7$ and it implies narrow resonances and a more efficient energy containment [15][16]. In the Results section (chapter 4) there is more information about the quality factor and its obtention for experimental purposes. In terms of wavelength, the quality factor is obtained with the wavelength of the center of a resonance divided by the full width at half maximum (FWHM).

Another important parameter, also more extended in chapter 4 below, is the Free Spectral Range (FSR). As the resonance condition is integer-dependent, the ring must support multiple resonances; the spacing between resonant wavelengths is the FSR:

$$FSR = \frac{c}{n_g \cdot L},$$
(2.5)

where c is the speed of light in free space, n_g is the group index and L is the optical resonator's length. The FSR determines the spacing between comb lines in soliton generation and must be large enough to be resolvable in the optical spectrum analyzer (OSA) [14]. In *Figure 6* there is an image representation of the FSR and the FWHM.

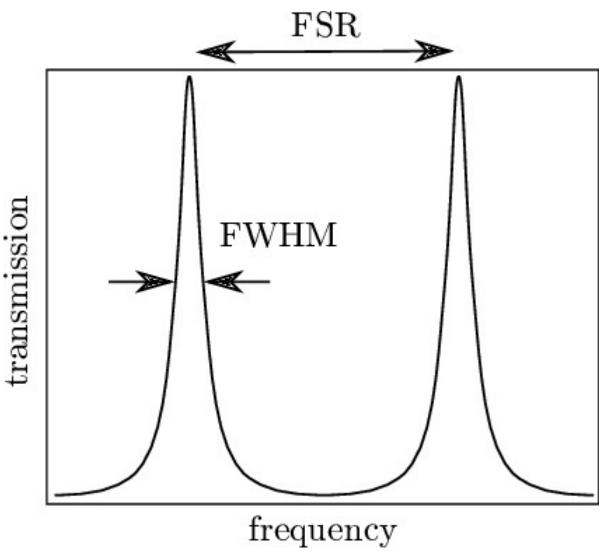

Figure 6. Schematic representation of the FWHM of a resonance and the FSR (Image extracted from Ref. [17])

2.2 Temporal solitons (frequency combs)

2.2.1 Kerr effect

The Kerr optical effect is a third-order nonlinear phenomenon in which the refractive index of a material changes in response to the intensity of the propagating light. This effect is described by the following equation:

$$n = n_0 + n_2 I,$$
(2.6)

where n_0 is the linear refractive index, n_2 is the nonlinear index coefficient (positive in most dielectrics), and I is the intensity of the light. As the intensity increases, the refractive index of the device increases accordingly, modifying the light phase and leading to intensity dependent phase shifts [18].

In microring resonators this effect is particularly important because the high Q factor and small mode volume lead to intense intracavity fields. Some phenomena that can be driven by the Kerr effect are: self-phase modulation, cross-phase modulation, four-wave mixing, optical bistability and dissipative Kerr soliton (DKS) formation. One of the most relevant consequences of the Kerr effect in resonators is the optical bistability and resonance shift.

As the refractive index increases with intracavity power, the resonance effectively shifts towards longer wavelengths, similar to the shift in the thermo-optic effect, but arising from an instantaneous and non-thermal origin. If the laser wavelength is scanned across a resonance, this shift can cause the system to exhibit step like spectra indicating the presence of multiple stable intracavity states [19].

This bistability is fundamental for the formation of dissipative Kerr solitons, which require a stable balance between dispersion, Kerr nonlinearity, loss, and external driving. When operating under appropriate input power conditions, the system can enter a regime where temporal solitons form spontaneously within the resonator. These solitons manifest in the spectral domain as optical frequency combs with a line spacing that is well defined and a characteristic sech^2 spectral envelope [20] [21]. This type of spectrum with the frequency combs can be seen in *Figure 7*.

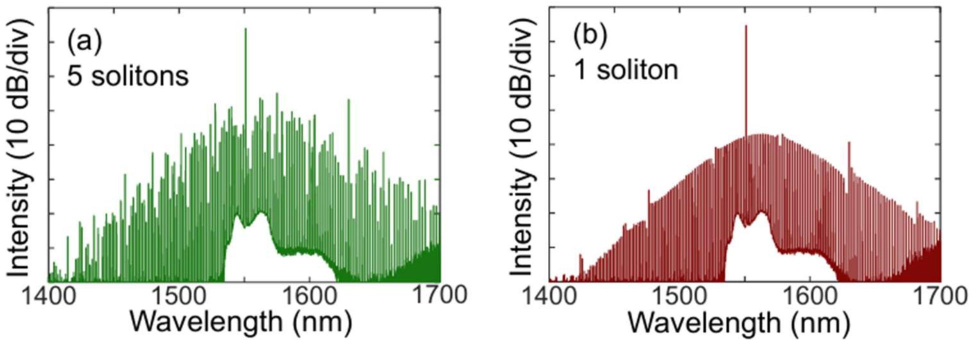

Figure 7. Spectra of a) multi-solitons, b) single-soliton with the characteristic $sech^2$ envelope (Image extracted from Ref. [21])

The Kerr effect is very fast and coherent, making it ideal for applications such as supercontinuum generation, all-optical switching, and on-chip comb sources. High-Q resonators with low losses can reach this nonlinear regime efficiently in silicon nitride [21].

2.2.2 Temporal soliton formation and optical frequency combs

In high-Q microresonators, the interplay between nonlinear Kerr effects, group velocity dispersion (GVD), cavity losses, and continuous-wave (CW) laser driving can lead to the formation of stable, self-localized waveforms known as dissipative Kerr solitons (DKS). These solitons are temporal pulses that circulate inside the resonator, maintaining their shape due to a balance between nonlinear effects, dispersion, energy input, and dissipation [19].

To form temporal solitons, the system must operate in the anomalous dispersion regime. That is where shorter wavelengths travel faster than longer ones: $\beta_2 < 0$ (β_2 is the second order dispersion coefficient). Additionally, the input power must exceed a threshold level to initiate phase modulation induced by Kerr effect [22][23].

The theoretical framework describing soliton dynamics in microresonators is the Lugiato–Lefever Equation (LLE), a nonlinear Schrödinger-type equation that describes the evolution of the field envelope inside the cavity deduced by Chembo and Menyuk [24][25]:

$$\frac{\partial E(t,x)}{\partial t} = \left[-\alpha - i\delta_0 + iL\frac{\beta_2}{2}\frac{\partial^2}{\partial x^2} + i\gamma L|E|^2\right]E + \sqrt{\theta}\,E_{in} \tag{2.6}$$

Here, E is the intracavity field envelope, δ_0 is the cavity laser detuning, γ the Kerr nonlinear coefficient, L is the cavity length and E_{in} is the amplitude of the input field [24].

In the spectral domain, the soliton manifests as a frequency comb: a series of equally spaced spectral lines whose separation is the FSR of the resonator. These combs typically display a characteristic sech^2-shaped spectral envelope, corresponding to the Fourier transform of the temporal soliton pulse [22].

The transition to the soliton regime often occurs after a chaotic behavior of the system, where the intracavity field fluctuates due to thermal and nonlinear effects. In particular, the thermo-optic effect can shift the cavity resonance dynamically, complicating soliton access if it's not managed properly. The thermo-optic consists of a change in the refractive index due to temperature increase from absorbed optical power, it is studied in more detail in chapter 4.

Once a stable soliton state is reached, it is usually observed as a distinct transmission step in the resonator's output, and the comb becomes visible on the OSA. In multi-soliton states, several pulses circulate simultaneously, resulting in modulated or structured combs due to interference effects [26][27].

Temporal Kerr solitons in Si_3N_4 microring resonators have demonstrated reliable, chip-scale sources of frequency combs for multiple applications, including optical clocks, spectroscopy, high speed data transmission and quantum photonics [19][27].

Chapter 3. EXPERIMENTAL CHARACTERIZATION

The following content describes the experimental characterization 3 carried out during this project. It begins with a detailed description of the experimental setups used for both transmission and reflection measurements, including all their optical components and their configuration. Then there is a description of the optical alignment, highlighting the steps required to achieve optima coupling between the input and output fibers and the waveguides of the chip. Finally, the physical characteristics of the sample with the PIC are described.

3.1 Experimental setups

This section presents the experimental setups used to obtain the results presented in this work. The first one, is a horizontal setup used for the measurements made in transmission, it was used for the characterization of the resonances of the rings and for the polarization study. This setup consists of different optical components as can be seen in *Figure 8.*

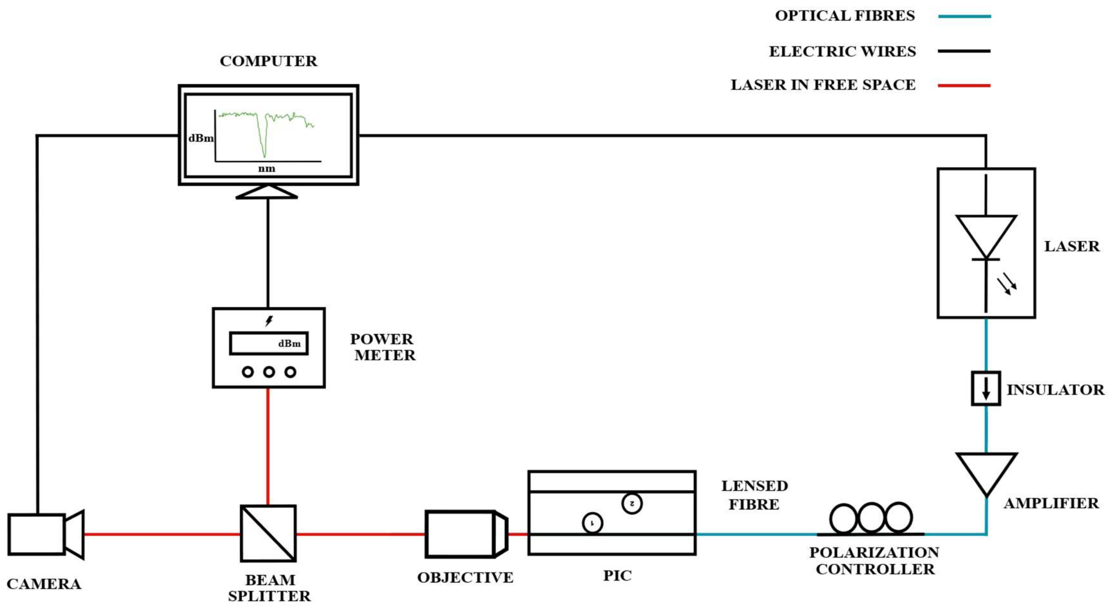

Figure 8. Schematic of the horizontal experimental setup (transmission)

First, as the light source we use a tunable Keysight Agilent 8164B laser approximately in the 1530 to 1570 nm range, with a minimum pitch of 0.001 nm. This laser is connected to a PriTel FA-30 Erbium- Doped Fibre Amplifier (EDFA), through an insulator, in order to achieve higher input powers. The EDFA has pump current from 0 to 4,99 A. The lensed fibre and the objective are mounted on positioning platforms that allow precise alignment thanks to their mobility in the X, Y and Z directions. The sample, which contains a PIC with two microring resonators and two waveguides, is placed on a holder that also allows movement, but only along the X and Z axes. The sample is held in place by air suction. For alignment, an infrared camera (Xenics Xeva-6685) is used, while the output power is measured using an optical power meter (ANDO AQ2140), that receives the power signal in dBm. Both devices receive the signal from the objective via a beam splitter. The laser can be operated locally through the device's front panel; however, it is usually controlled via the computer, which also receives the power measurements from the power meter and the images from the camera. In *Figure 9* we can see a photo of the setup and a close-up of the sample aligned with the objective and the optical fibre.

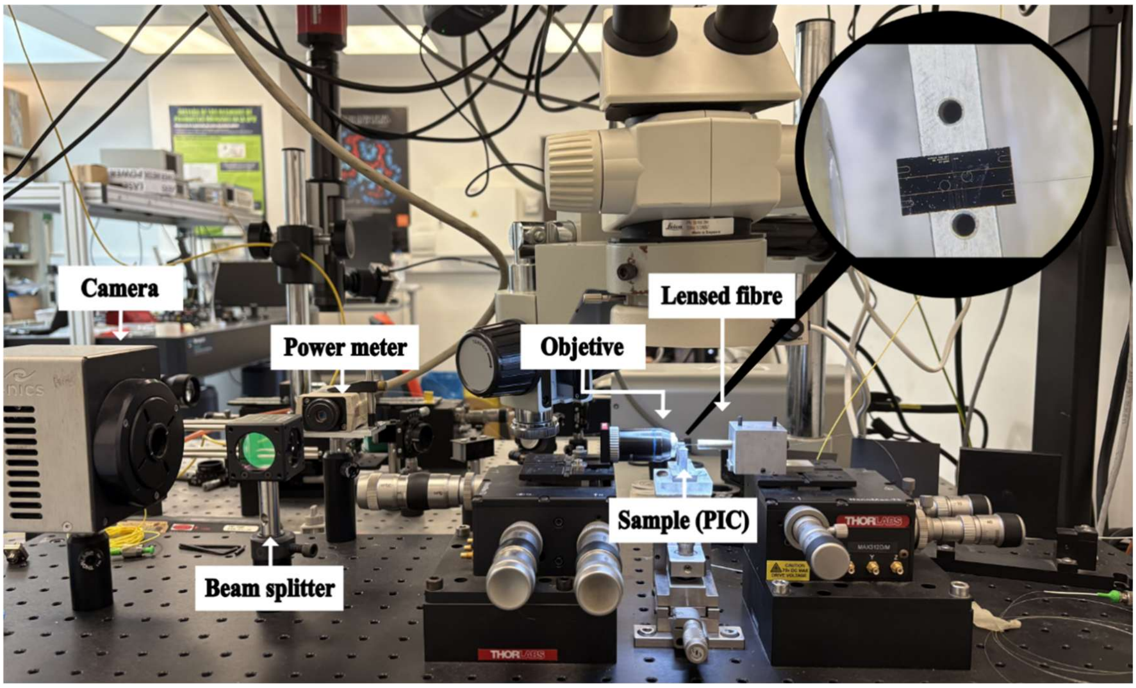

Figure 9. Photo of the first experimental setup with a close-up of the chip

The second experimental setup, shown in *Figure 10*, is identical to the other one with the addition of a few components that are made to be able to take measurements in reflection and connect with the optical spectrum analyzer (OSA) and the oscilloscope. The first component added is an optical circulator, which is placed between the output of the EDFA and the lensed fiber. It directs the signal from the laser, amplified by the EDFA, from port 1 to port 2, sending light into the sample through the polarization controller. The reflected signal returning from the sample travels from port 2 to port 3 and ends in a fibre coupler that splits the signal 50/50. Half of the reflected signal is directed to an optical spectrum analyzer (OSA) ANDO AQ6317C, while the other half is sent to the power meter that is connected to the oscilloscope Keysight DSO81204B. In the oscilloscope we receive the spectrum of the resonances in reflection and the OSA measures and displays the power distribution over a wavelength range [28]. In this setup we also used a different tunable laser TSL-570 working in a range from 1480 to1640 nm, with a smaller pitch of 0.1 pm, to better study the thermo-optic effect. The other components are similar to the ones in the other setup, but some are not exactly the same: the power meter is a Newport 1930C and the infrared camera is a Xenics Xeva-1508, but they perform the same function as in the previous setup. *Figure 11* shows a photo of this second setup with the new components needed to connect with the OSA and the oscilloscope.

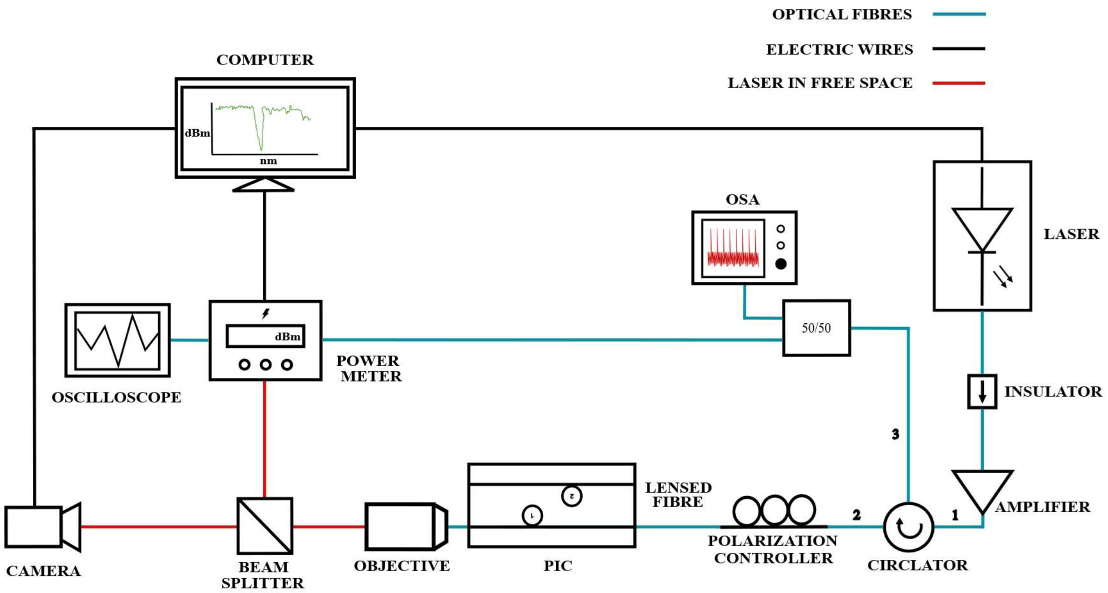

Figure 10. Schematic of the second horizontal experimental set-up (reflection)

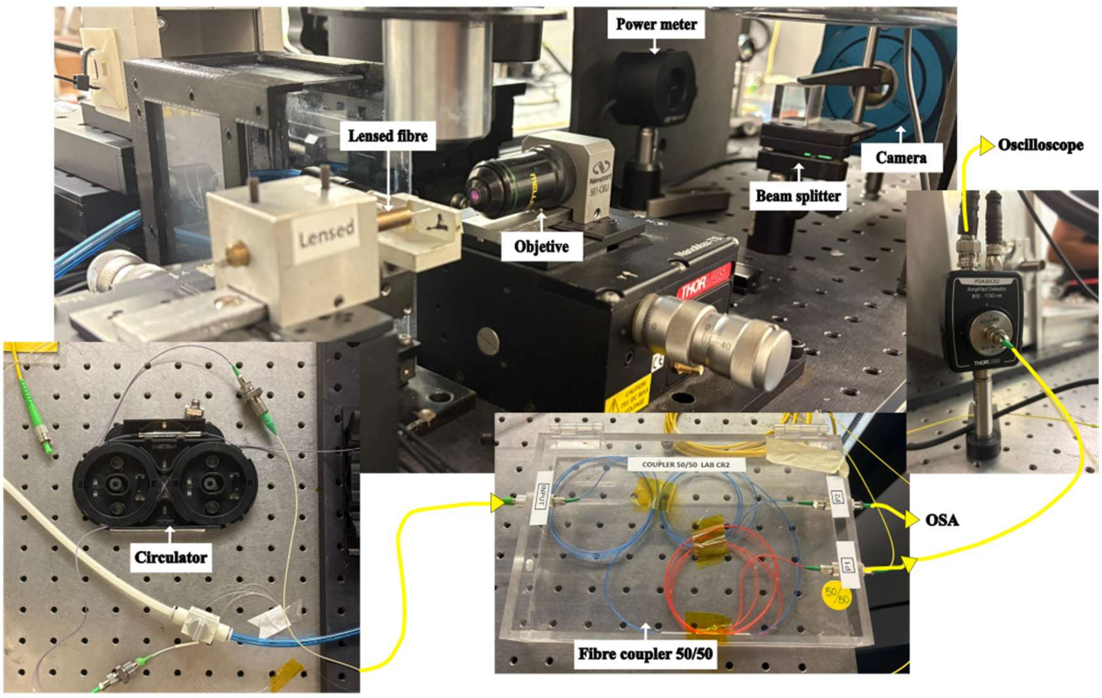

Figure 11. Photo of the second experimental setup with images of the circulator and the fibre coupler (50/50) which connect the setup with the OSA and the oscilloscope that are on another workbench

3.2 Alignment process

Before starting the measurement process, it is essential to align all optical components and optimize the output signal in order to achieve the maximum possible power. This process ensures that the system operates under optimal conditions, minimizing losses and allowing accurate data acquisition.

We begin with the fibre-objective alignment. Using the positioning platforms, both elements are brought close together by adjusting their position along the X, Y, and Z axes until a light spot becomes visible on the screen. Once we've found the light spot, we optimize the output signal trying to obtain maximum transmission by slightly moving the objective or the fibre. Proper alignment is confirmed by observing a sharp and centered spot on the camera and by ensuring that the power meter registers the highest possible optical power. *Figure 12. a)* shows a schematic of the process and the elements involved in it.

Next, the sample must be aligned with the fibre and the objective. To do so, the lensed fibre is first separated from the objective, and the sample is positioned between the other two components. The fibre is then slightly separated and lifted above the sample to obtain an image of the light diffraction patterns through the objective (*Figure 12. b)*). Then we move the objective vertically until the diffraction pattern only occupies half the screen, and along the Y axis to sharpen the image of the lines (*Figure 12. c)*). Subsequently, the lensed fibre is gradually lowered (Z axis) while we watch the diffraction fringes get wider until they disappear from the screen. After that, we only have to move the objective in the X direction until we find a light spot as can be seen in *Figure 12. d)*. Finally, there are only some final adjustments left to make to the fibre, the objective and the polarization controller to maximize transmission, as verified by the power reading at the output.

An optical microscope positioned above the setup is also used to assist in the alignment process. For safety reasons, the laser remains off while using the microscope, even though the wavelength employed (around 1550 nm) is in the infrared range and is typically considered eye-safe at the power levels used for alignment as long as the EDFA is not connected.

In *Figure 13* we can see the result of both the fibre-objective and the fibre-sample-objective alignment.

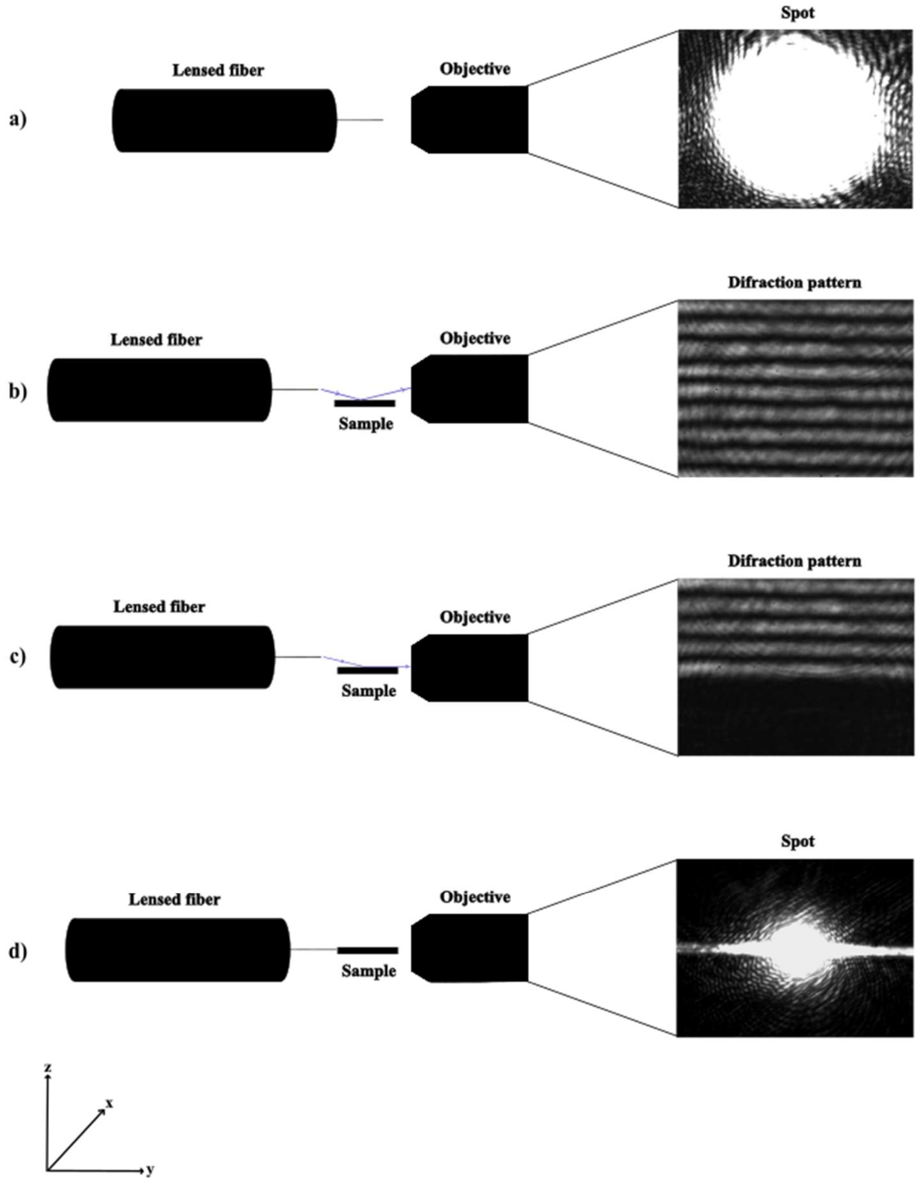

Figure 12. Schematic of system alignment process

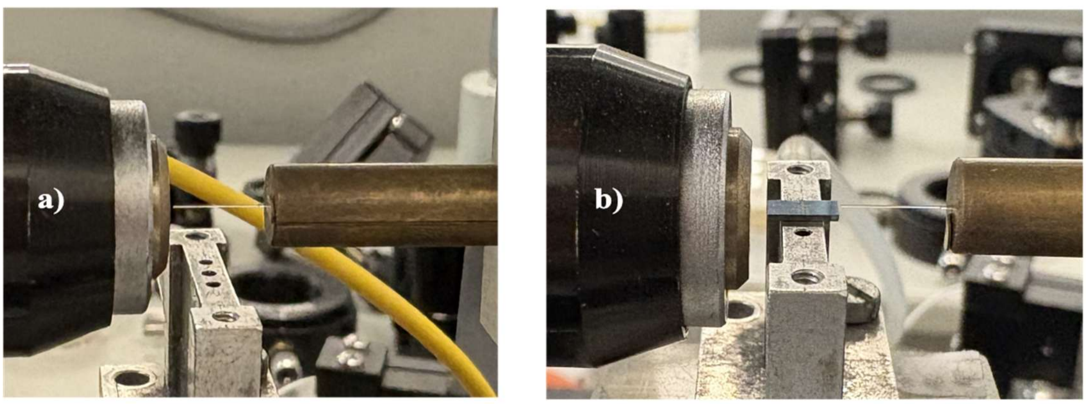

Figure 13. a) Photo of the objective and the fibre aligned b) Photo of the objective, sample and fibre aligned

3.3 The sample

The sample used in the experimental measurements consists of a silicon nitride (Si_3N_4) PIC fabricated on a planar chip. This material is well known for its low propagation losses and its wide optical transparency window in the visible and the infrared range. The chip includes two identical microring resonators coupled to a straight waveguide each. The rings are designed for ultralow loss operation in the telecom C-band and as optical cavities they are excellent for optical filtering or for the study of nonlinear phenomena [29].

In *Figure 14* there is a microscope image of the PIC where the waveguides and the rings can be clearly identified. The microrings are used to filter specific wavelengths based on their resonance, while the waveguides serve as input and output channels for light propagation. The waveguides are connected to edge couplers on both sides of the chip, allowing for efficient alignment with the lensed fiber and the objective lens system used in the setup. As mentioned before, the sample is mounted on a holder that allows movement in two directions to help with the alignment process.

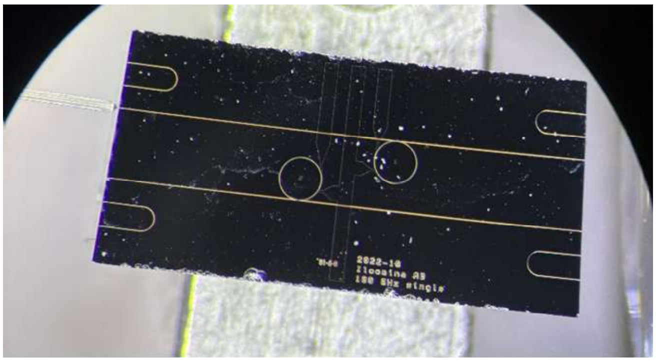

Figure 14. Microscope image of the PIC

The total chip size is quite small, approximately 3x5 nm^2. The microring radius is around 230 µm and the distance between the waveguide and the resonator is optimized for evanescent coupling. The waveguide width is around 5 µm and so is the ring's. There are no electrical contacts or active elements present in this sample, as the experiment is based only on passive optical components that guide and filter light without the need for electrical control. An image of the chip extracted from the datasheet provided by Iloomina, the supplier, can be seen in *Figure 15*.

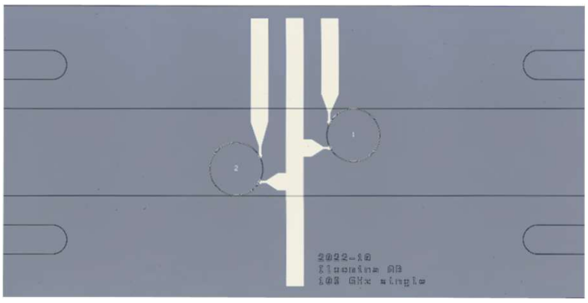

Figure 15. Image of the chip from the datasheet by the supplier (appendix A)

In *Figure 16* there are close-ups of the rings and the waveguides, made with an optical microscope Axiolab 5 with different magnifying lenses (10x, 50x) and the Axiocam 208 color. The measurements of the width of the waveguides and the rings, and the radius of the rings were made using these images and DigitalMicrograph, a widely used software for analysis and processing of images and spectra.

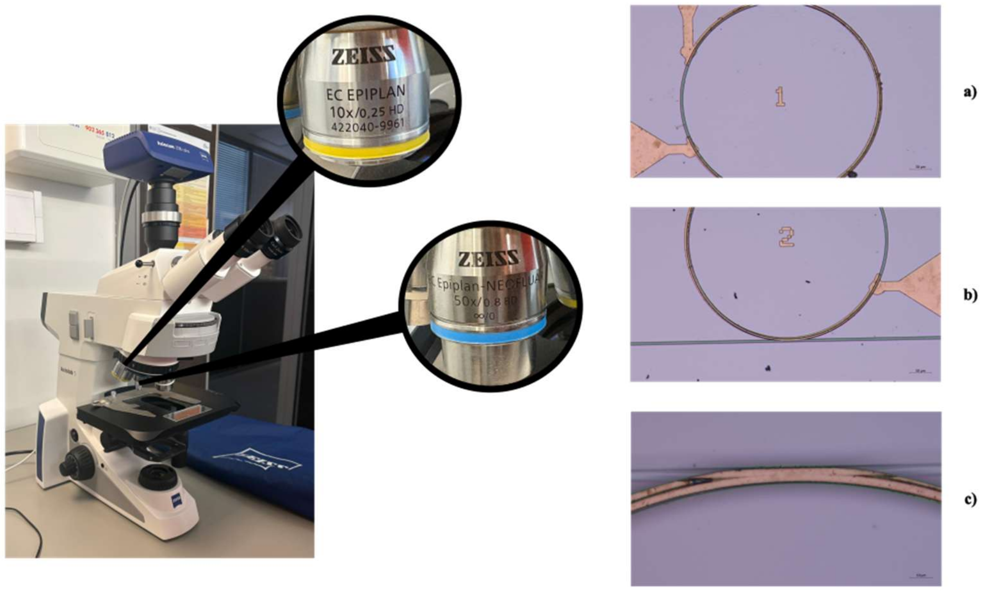

Figure 16. Optical microscope Axiolab 5 with the 10x and the 50x objectives. a), b) Close-ups of the two rings made with the 10x objective. c) Close-up of one of the rings and its waveguide made with the 50x objective

Chapter 4. RESULTS

In this chapter, we present all the results obtained from the experimental work carried out throughout the project. These results are presented in a specific order to reflect the progression of the experiments and will be interpreted later in the corresponding section.

4.1 Characterization of the resonances

The first contact with the experimental measurements was making different wavelength sweeps to find the optical resonances of the microrings. These measurements were made in transmission and with them we were able obtain the quality factor (Q factor) and the free spectral range (FSR) of the ring resonators.

4.1.1 Quality factor

The Q factor is a measure of the frequency selectivity of the ring resonator. It's a dimensionless parameter that quantifies how effectively a resonator stores optical energy relative to the rate at which it loses it. It can be obtain for experimental purposes as:

$$\boldsymbol{Q = \frac{\lambda_0}{FWHM},} \quad \textbf{(4.1)}$$

where FWHM is the full width at half maximum of the ring resonance and λ_0 is the wavelength value at the center of the resonance. A high Q factor indicates narrower resonances and lower intrinsic losses, which are crucial for enabling nonlinear effects and for supporting stable soliton formation in microresonators [30]. We used Origin software to obtain the Q factor by processing the data from the experimental work. In *Figures 17, 18* and *19*, a resonance is displayed along with a Lorentzian fit, performed using Origin software, to extract the quality factor of our rings.

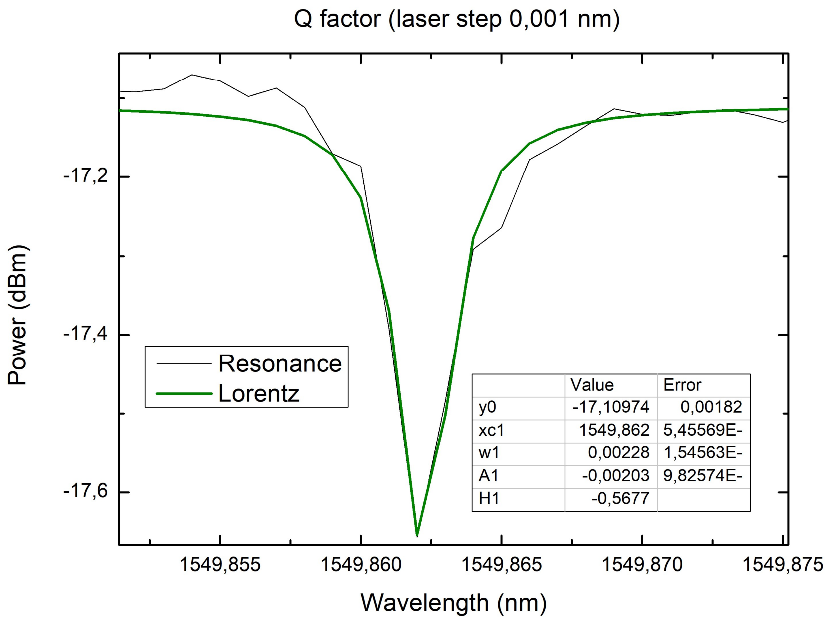

Figure 17. Resonance spectrum 1 with Lorentzian fit and corresponding fit parameters from Origin software

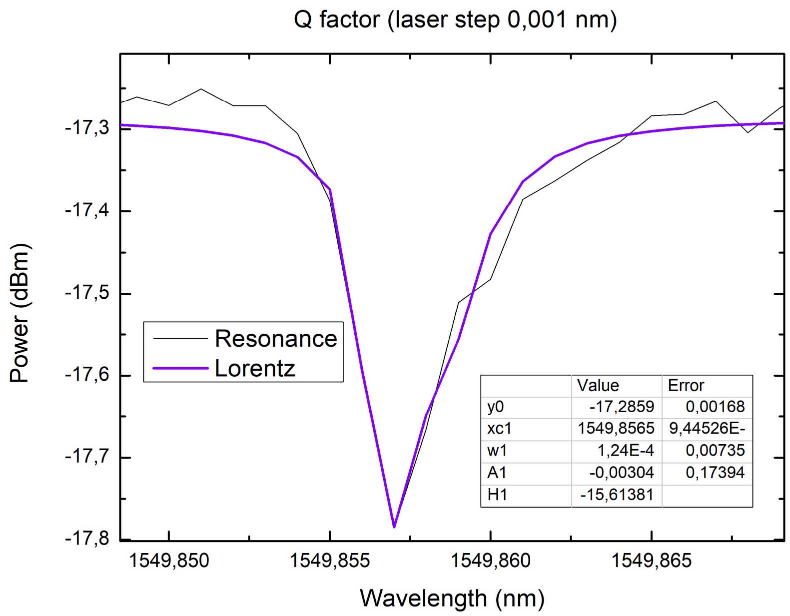

Figure 18. Resonance spectrum 2 with Lorentzian fit and corresponding fit parameters from Origin software

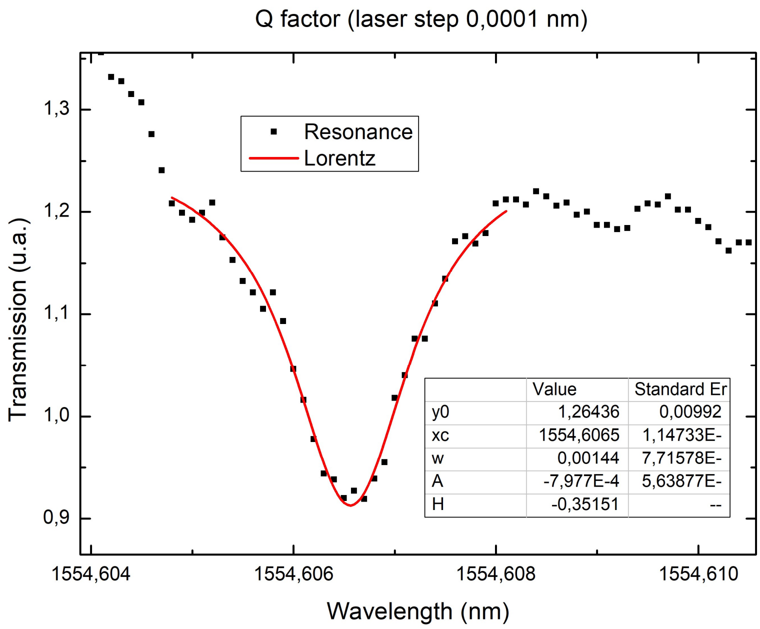

Figure 19. Resonance spectrum 3 with Lorentzian fit and corresponding fit parameters from Origin software

From the previous plots, we can obtain the quality factors of our sample:

$$Q_1 = \frac{1549.8622\ nm}{0.00228\ nm} = 6.798 \cdot 10^5,$$

$$Q_2 = \frac{1549.8565\ nm}{0.00735\ nm} = 2.109 \cdot 10^5,$$

$$Q_3 = \frac{1554.60656\,nm}{0.00112\,nm} = 1.388 \cdot 10^6.$$

These values were extracted directly from the Lorentzian fit in Origin, where 'xc' corresponds to the central wavelength λ_0 and 'w' denotes the FWHM.

To efficiently generate temporal solitons in silicon nitride ring resonators, a high Q factor is essential. Usually, a Q factor ≥ 10^6 ensures low enough losses for enabling Kerr nonlinearities and soliton formation [16]. We achieved a Q factor of approximately 1.4·10^6 in the third spectrum, which is considered a high value and should allow for the observation of a frequency comb spectrum. The other two values are a bit lower due to the step of the laser that is less precise.

4.1.2 Free spectral range

In addition to the quality factor, the free spectral range (FSR) also plays a crucial role in the resonator's behavior. To generate frequency combs in Si_3N_4 microring resonators it is important that the resonator's FSR allows the spectral lines to be clearly resolved. An FSR in the range of 90-200 GHz for microresonators is well suited for generating combs detectable with a standard OSA [31].

The free spectral range of our rings fits in that range and can be found in the datasheet provided by the supplier; it is 100 GHz (appendix A). To convert this frequency range to wavelength we use the following formula:

$$\Delta\lambda = \frac{c}{{f_{center}}^2}\,\Delta f, \tag{4.2}$$

where the center frequency is:

$$f_{center} = \frac{c}{\lambda_{center}} = \frac{3 \cdot 10^8\ m/s}{1550 \cdot 10^{-9}\ m} = 1.935 \cdot 10^{14}\ Hz. \tag{4.3}$$

The FSR in wavelength is:

$$\Delta\lambda = \frac{3 \cdot 10^8 m/s}{(1.935 \cdot 10^{14} Hz)^2} \cdot 100 \cdot 10^9\ Hz = 8 \cdot 10^{-10}\ m = 0.8\ nm. \tag{4.4}$$

This means that when we make a wavelength sweep the resonances will be separated by around 0.8 nm. In *Figures 20* and *21* there are plots of two different sweeps where the ring's resonances can be clearly identified and the FSR, calculated as an average of the distances between resonances, is also shown. In the first plot the average FSR is around 0.788 nm and in the second one around 0.797 nm, both values are very similar to the theorical value of 0.800 nm calculated above.

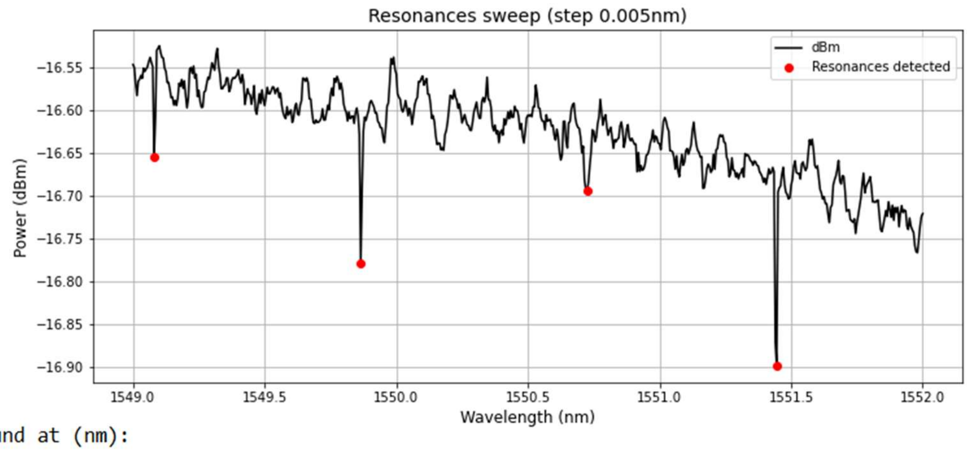


```
Resonances found at (nm):
1549.080
1549.865
1550.725
1551.445
Average FSR (nm): 0.7883333333333363
```

Figure 20. Plot of a sweep from 1549 to 1552 nm with the resonances indicated and the average of the FSR

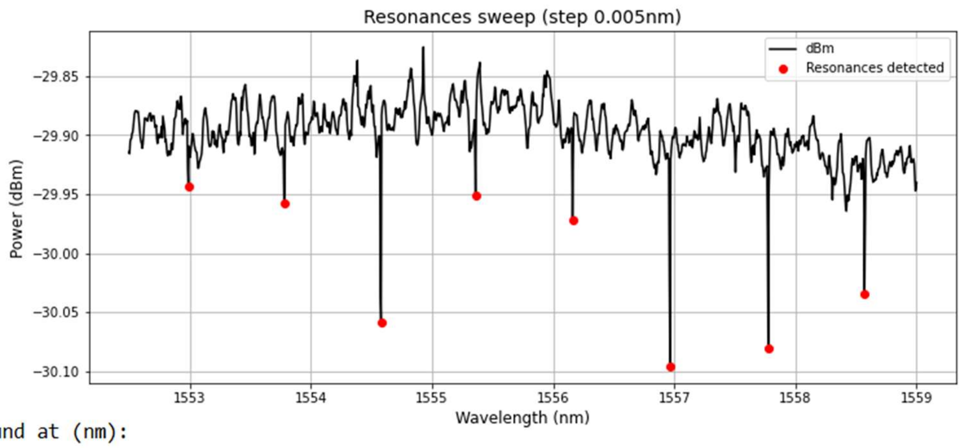


```
Resonances found at (nm):
1552.990
1553.780
1554.580
1555.360
1556.160
1556.965
1557.775
1558.570
Average FSR (nm): 0.7971428571428467
```

Figure 21. Plot of a sweep from 1552 to 1559 nm with the resonances indicated and the average of the FSR

4.2 Polarization study

In order to study the polarization dependence of the system, a polarization filter was added to the experimental setup between the objective and the beam splitter (*Figure 22*). This component allows the transmission of either the TE (transverse electric) or TM (transverse magnetic) modes of the input light. The polarizer has a wheel with angular markings that enables precise control of the polarization state. Specifically, if we want to transmit only the TM mode we set the wheel to 0º, while at 90º it only allows the TE mode to pass.

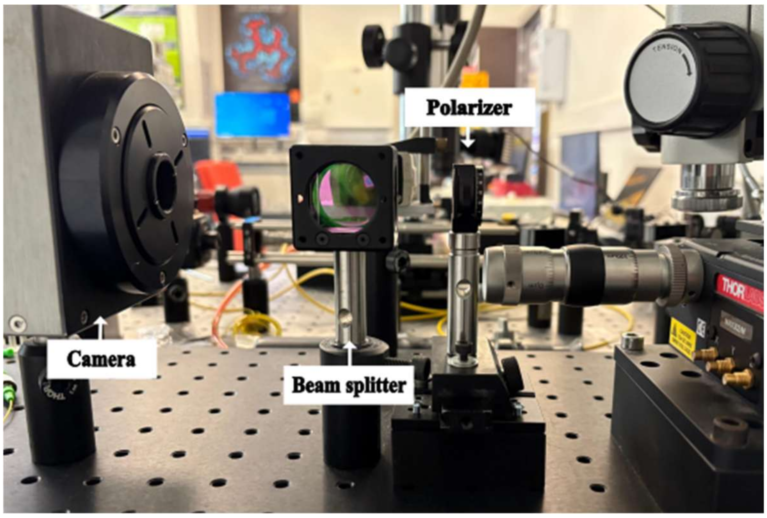

Figure 22. Photo of the polarizer in the experimental setup

In *Figure 23* there is a plot of the resonances without the polarization filter, with it in mode TE (90º) and with it in mode TM (0º). In *Figure 24,* we can also see some resonances with the polarizer set to TE mode and then to TM mode. Based on these results, resonances are present under all three conditions: with the polarizer set to transmit TE, to transmit TM, and without the polarizer. This indicates that the sample supports both polarization modes, and we can conclude that the system exhibits hybrid polarization behavior. For this reason, and to avoid unnecessary losses, the polarizer was not used in the rest of the measurements.

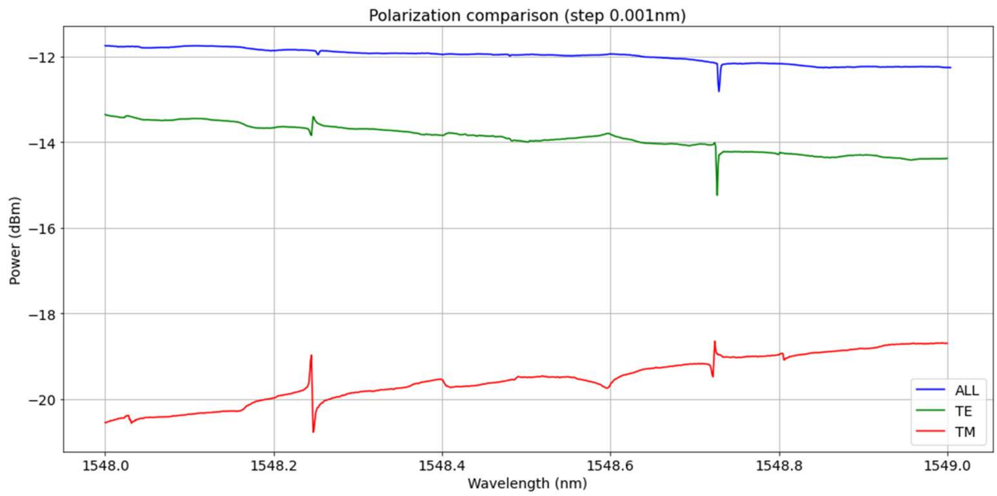

Figure 23. Plot of two resonances with the polarizer set to TE mode, to TM mode, and without polarizer

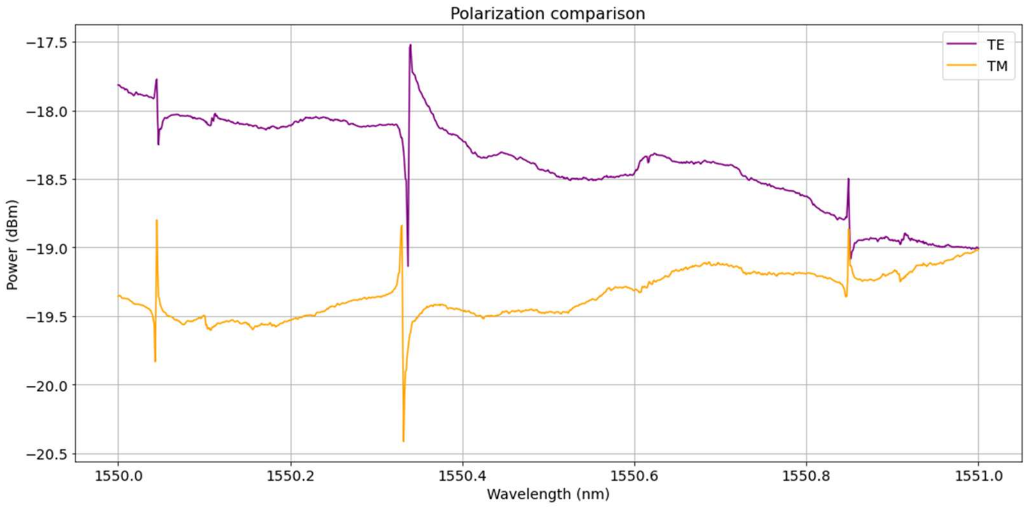

Figure 24. Plot of two resonances with the polarizer set to TE or TM mode

Additionally, observing the resonances under both TE and TM polarization states, our measurements revealed the presence of Fano resonances (*Figure 25* and *26*). These symmetric resonances occur due to the interference between a discrete resonance (from the microring) and a continuous background (direct transmission through the waveguide), and they are characteristic of resonant structures such as our ring resonators. The presence of symmetric Fano resonances under both TE and TM excitation confirms the hybrid polarization behavior of the chip and highlights the potential for high-sensitivity applications such as nanophotonics and sensing [32].

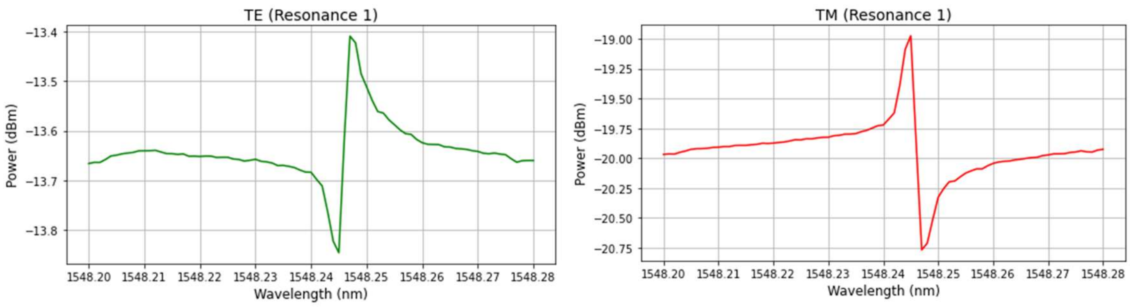

Figure 25. Resonance 1 close-ups from Figure 21 in TE and TM mode

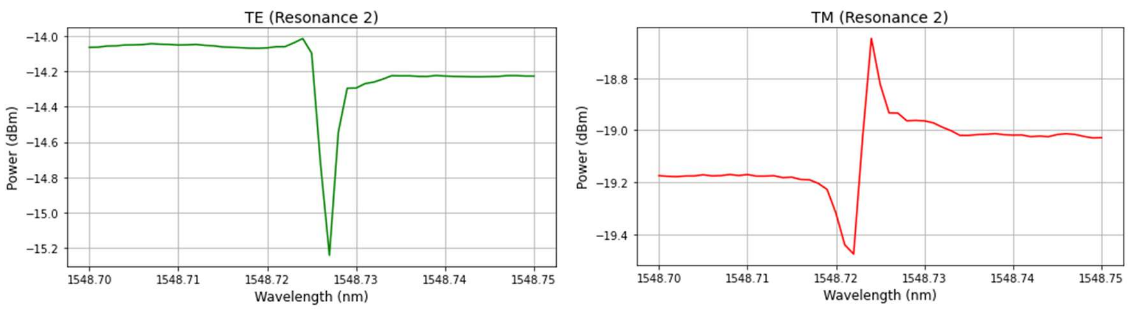

Figure 26. Resonance 2 close-ups from Figure 21 in TE and TM mode

4.3 Towards the observation of temporal solitons

4.3.1 EDFA amplification test

Before starting the main measurements using the EDFA, we performed some tests to verify that the amplifier was functioning correctly. For this purpose, a portable optical power meter was placed at the output of the EDFA, which receives the signal from the tunable laser. During the tests, the pump current of the EDFA was gradually increased, and the output power was recorded.

As shown in *Figure 27*, the output power remains low and nearly constant for small pump currents, but once a certain threshold is exceeded, it begins to increase rapidly and almost linearly. This confirms that the EDFA amplifies the input signal properly.

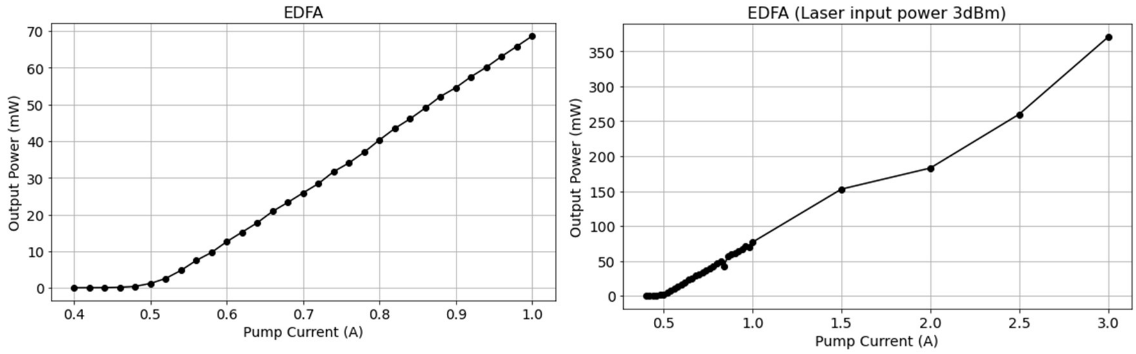

Figure 27. EDFA characterization curves. The plot on the left is taken with a laser input power of 0 dBm while the plot on the right has a laser power input of 3dBm

4.3.2 Thermo-optic effect

In order to explore the possibility of observing temporal solitons in our ring resonators, we first performed a set of measurements to verify the presence of the thermo-optic effect in the sample. This effect occurs when the Si_3N_4 waveguide is illuminated with intense light, due to the optical absorption of the photonic structure (ring resonator) that leads to heat generation and rises the local temperature. This modifies the material's refractive index and influences the propagation of light through the material [33].

To study this, we gradually increased the input power with the EDFA and monitored the position and shape of the resonances. As shown in *Figure 28* and *29* the resonances progressively shifted towards longer wavelengths (redshift) as the input power increased, which is a clear indication of the thermo-optic effect and is typically the first nonlinearity to appear in these photonic devices.

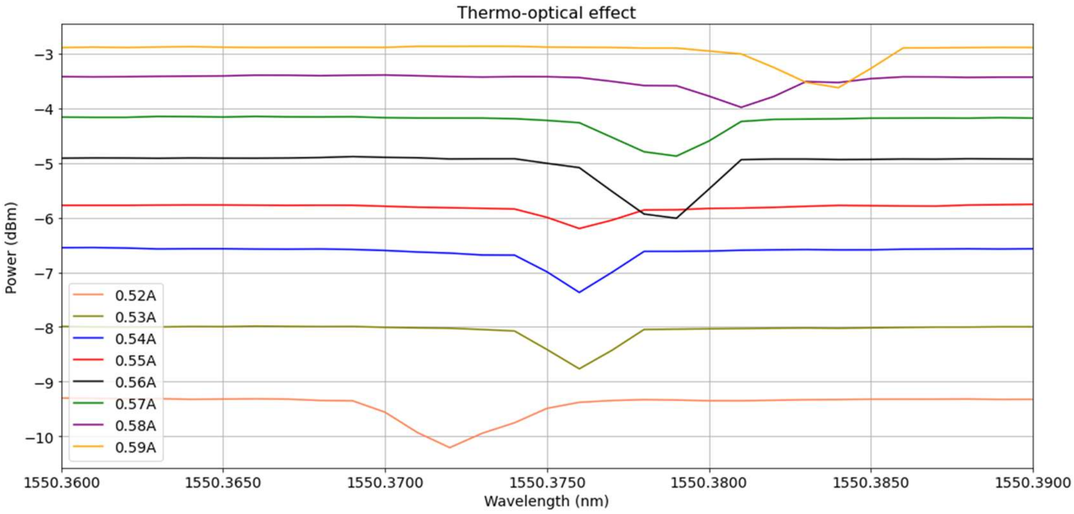

Figure 28. Resonance shifts as a function of the EDFA's pump current. Laser step 0.001nm

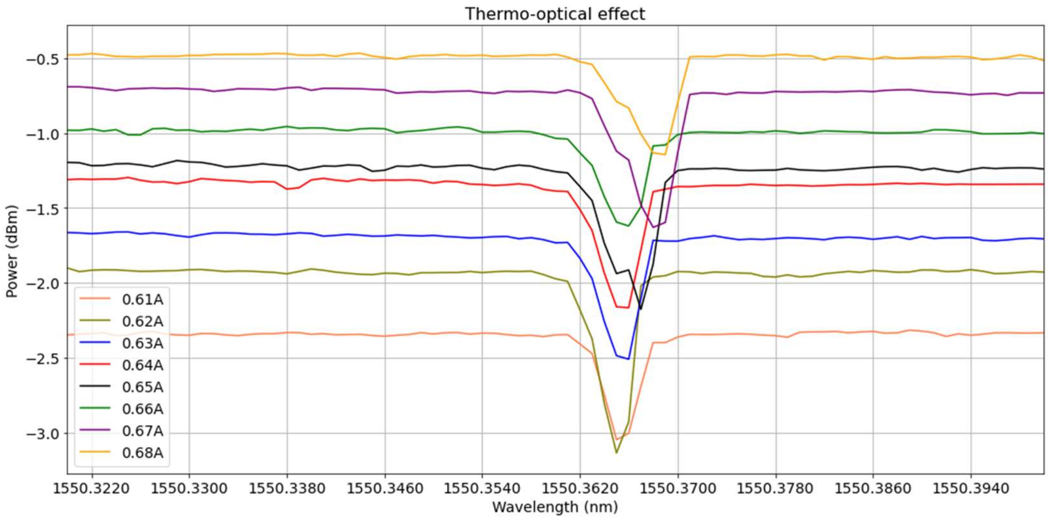

Figure 29. Resonance shifts as a function of the EDFA's pump current. Laser step 0.001nm

At this point we changed to the second setup (reflection), to be able to get a clearer vision of the resonances. We continued to increase the input power, and the dips associated with the resonances started to transform into abrupt steps. In *Figure 30*, there is a step-shaped resonance in which the sharp drop of the step can be clearly seen. This behavior is commonly associated with nonlinear resonance bistability and is considered a precursor to the formation of temporal cavity solitons in microring resonators [31].

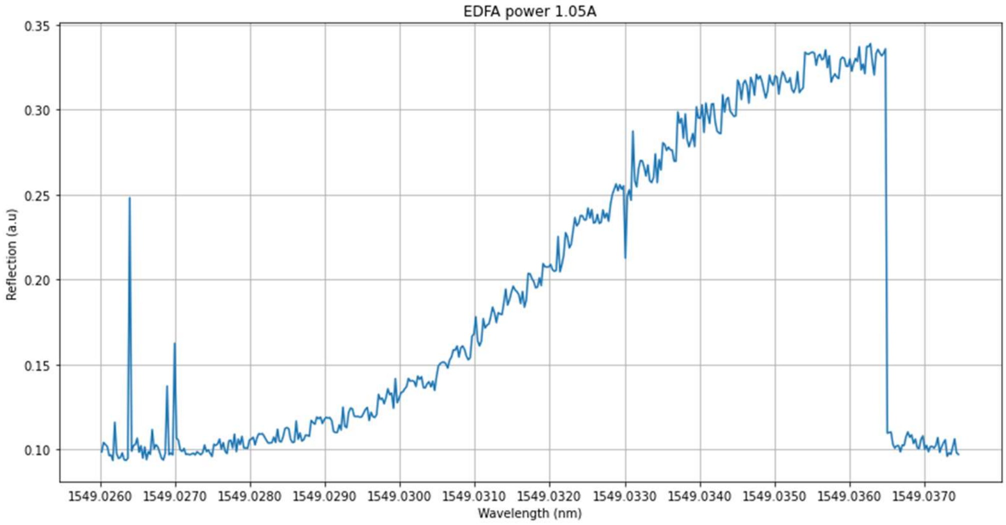

Figure 30. Step-shaped resonance at a high power (1.05A) measured in reflection. Parametric sweep from 1549.0260 to 1549.0380 nm, step 0.0001nm

In *Figure 31*, there is a series of spectra where the thermo-optic effect can be observed. The redshift of the resonance steps is clearly visible in most of the spectra, however, there are some deviations from the expected behavior. In a few cases the resonances appear to temporarily shift backwards before resuming their redshift, this is likely the result of some nonlinear effects such as thermal instabilities, the local saturation of the thermo-optic effect or fast Kerr nonlinearity [33][34].

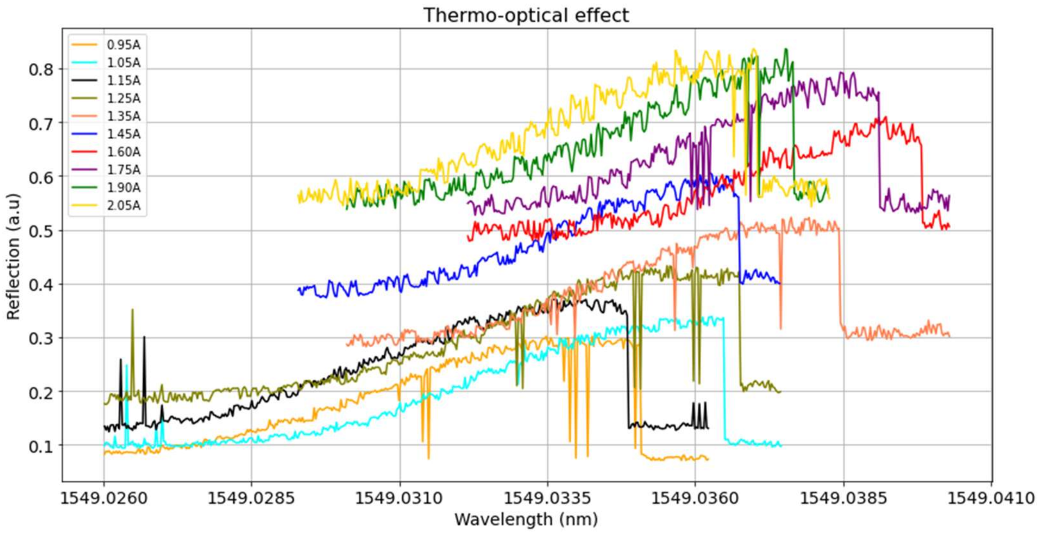

Figure 31. Spectra at increasing input powers from the EDFA showing thermo-optical effect. Laser step 0.0001 nm

This set of measurements serves as an essential step previous to the nonlinear regime necessary for soliton generation and helps map the power levels at which different optical phenomena occur in our sample.

4.3.3 Towards the observation of combs

Once the thermo-optic effect is studied, the next step is the observation of temporal solitons. For this purpose, we kept increasing the input power with the EDFA and started recording the spectra from the OSA. In *Figure 32* there is an OSA spectrum with a step of 0.01 nm and the laser fixed at a wavelength that we know is at resonance of 1549.0360 nm. In *Figure 33* there is another spectrum like the previous one but at a different wavelength and some other different parameters, and in *Figure 34* this same spectrum but limited to a smaller wavelength range. While taking the measurements with the OSA, to ensure that we are within the resonance we set the laser at a wavelength that is around the center of the peak of the resonance.

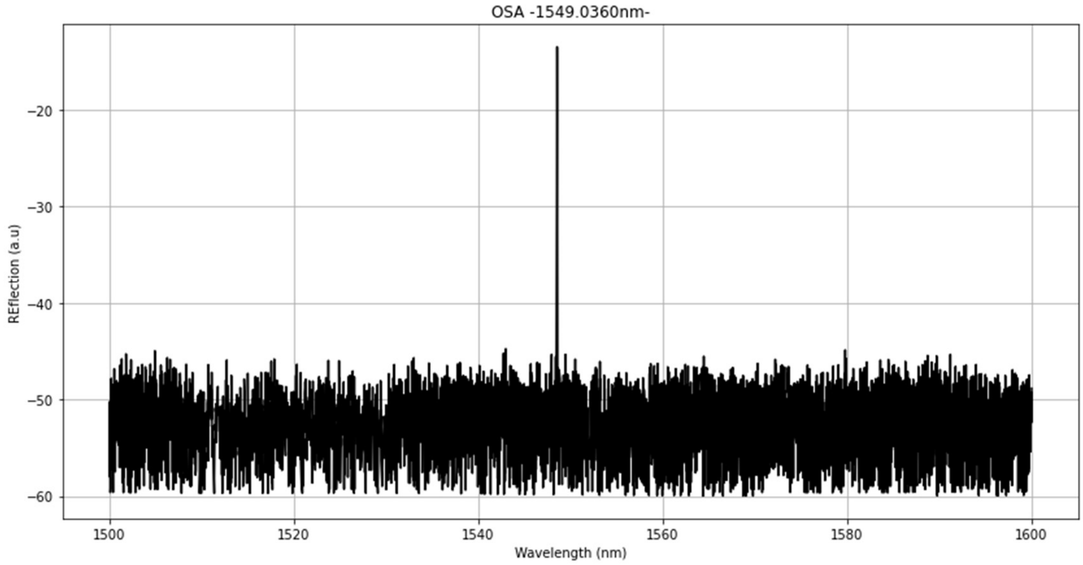

Figure 32. OSA spectrum from 1500 to 1600 nm with 0.01nm step and 1 accumulation, resonance at 1549.0360 nm

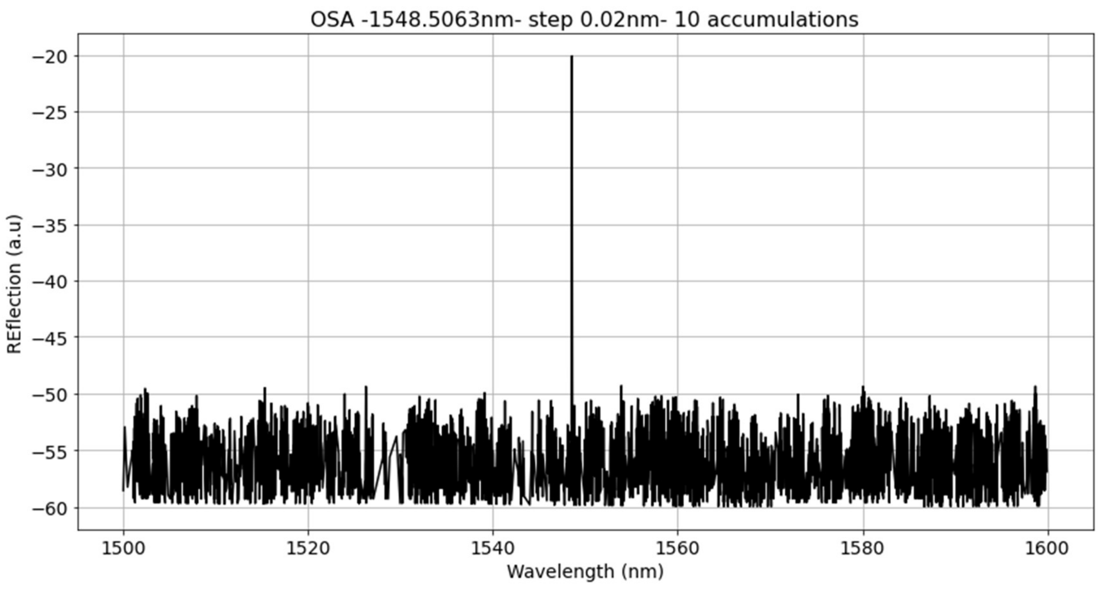

Figure 33. OSA spectrum from 1500 to 1600 nm with 0.01 nm step and 10 accumulations, resonance at 1548.5063 nm

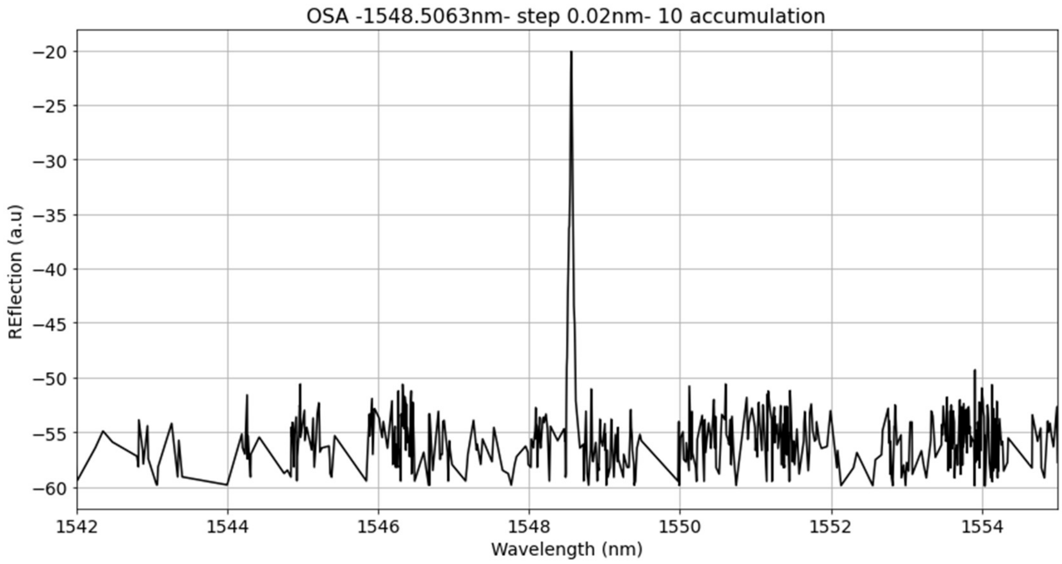

Figure 34. Closeup of plot from Figure 31

The next step towards the observation of temporal solitons involves gradually increasing the optical power from the laser, as we did when observing the thermo-optic effect, however now as we increase the input power we must check the spectra that appears in the OSA. As the power rises, thermal nonlinearities dominate initially, but at a certain threshold, Kerr nonlinearities start to play a significant role. To detect the soliton formation, we perform spectral sweeps with the OSA while keeping the system in resonance and at high powers. If solitons form within the ring resonator, the output OSA spectrum will exhibit a frequency comb: a sequence of narrow, evenly spaced spectra lines across a broad wavelength range. In *Figure 35* there is an example of such frequency comb spectrum of the work by Herr et al., where the measured spectrum displays a smooth and symmetric envelope and a set of equally spaced spectral lines, as expected from a single dissipative Kerr soliton state. In our setup, scanning the OSA while increasing the input power and remaining in resonance would allow us to detect this comb structure, confirming entry into the soliton regime [19].

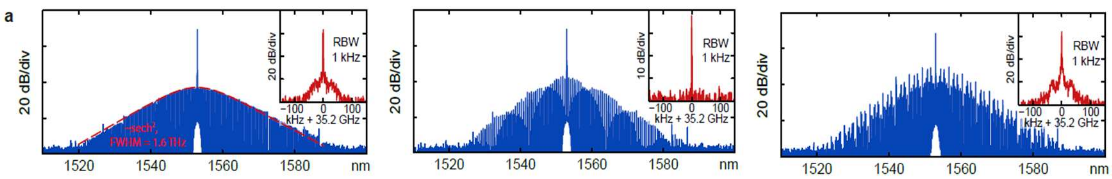

Figure 35. Optical spectra of three select comb states with one, two and five solitons respectively Iimages adapted from Ref. [33])

Although the setup was designed with the aim of reaching the temporal soliton regime, and the experimental work followed the established steps, it was ultimately not possible to observe the formation of optical frequency combs in our experimental setups. As the input power increased to the levels required for soliton formation, the optical fibres from the setup began to suffer from burning, resulting in a significant loss of signal. This prevented the acquisition of the comb-shaped spectra that required high powers.

Investigating the literature, we also discovered that in order to obtain frequency combs the measurements should have been made in transmission as in the first experimental setup. Nevertheless, these failed results highlight critical aspects of the experimental limitations and guide us to areas of improvement. Work is currently underway to optimize the setups, particularly in terms of power handling and fibre coupling stability, in order to enable stable operation at higher input powers and allowing successful observation of the formation of solitons in future experiments.

Chapter 5. CONCLUSION AND FUTURE WORK

This final degree project has presented the experimental characterization of a silicon nitride PIC containing waveguides and microring resonators, with the objective of exploring their linear and nonlinear optical behavior. Additionally, the optical setups were implemented and aligned for both transmission and reflection measurements. The characterization of both the sample and the experimental setups was accomplished, and we were able to obtain some important information from them, such as the microring's quality factor or the EDFA's behavior.

The thermo-optic effect was successfully observed through the shift of the resonance's wavelength with the increasing input power, and at high powers the steps started to appear in the spectrum as well, indicating the presence of nonlinear phenomena. Although the formation of temporal solitons and frequency combs was not achieved due to some setup problems like the damage of the fibres at high powers, the results confirmed that the system reaches the nonlinear regime under controlled conditions. This work has helped identify the challenges in coupling, thermal stability and power handling that must be addressed in future experiments to be able to observe dissipative Kerr solitons in microring resonators.

The future work will focus on optimizing the experimental setups to enable soliton formation in a more stable and reproducible way. This includes improving fibre coupling and cleaning techniques and exploring other methods of optimizing the experimental setups. Also, for the observation of optical frequency combs, the measurements with the optical spectrum analyzer will have to be taken in transmission. For this purpose, the experimental setup must change to measure fibre to fibre, instead of with the objective. This will allow us to make measurements in transmission with the oscilloscope and the OSA, and observe the generation of temporal solitons in the microring resonators.

The study of nonlinear phenomena in optical devices is still very relevant, as they offer valuable insights into complex light interactions and also promising opportunities for practical applications in areas such as optical communications and integrated photonics technologies. This shows there is still much research and experimental work to be done in this area and the optimization of the work carried out through this project is a step in that direction.

REFERENCES

[1] Yang, QF., Hu, Y., Torres-Company, V. *et al.,* "Efficient microresonator frequency combs," eLigth 4, 18, Oct. 2024. Available: https://doi.org/10.1186/s43593-024-00075-5 [Online].

[2] L. Chang, S. Liu, J.E Bowers, "Integrated optical frequency comb technologies," *Nature photonics* 16, 95-108, Feb. 2022. https://doi.org/10.1038/s41566-021-00945-1 [Online].

[3] United Nations, "Sustainable Development Goals," United Nations, https://www.un.org/sustainabledevelopment/sustainable-development-goals/ [Online].

[4] Newport Corporation, "Fiber Optic Physics," Newport, https://www.newport.com/n/fiber-optic-physics [Online].

[5] FiberLabs, "Optical Fiber," FiberLabs Glossary, https://www.fiberlabs.com/glossary/optical-fiber/ [Online].

[6] Lase Optics, "Lensed Fibers," Lase Optics Corporation, https://laseoptics.com/lensed-fibers/ [Online].

[7] Wikipedia contributors, "Fiber-optic communication," *Wikipedia, The Free Encyclopedia*, https://en.wikipedia.org/wiki/Fiber-optic_communication [Online].

[8] R. Paschotta, "Fiber Polarization Controllers," *RP Photonics Encyclopedia*, https://www.rp-photonics.com/fiber_polarization_controllers.html [Online].

[9] M. A. Butt, L. Kozlowski, M. Słowikowski, M. Juchniewicz, D. Drecka, M. Filipiak, M Golas, B. Stonio, M. Dudek, R. Piramidowicz, "Investigation of Modal Characteristics of Silicon Nitride Ridge Waveguides for Enhanced Refractive Index Sensing," *Micromachines*, 16(2), 119 Jan. 2025. https://www.mdpi.com/2072-666X/16/2/119 [Online].

[10] Wikipedia contributors, "Waveguide (optics)," *Wikipedia, The Free Encyclopedia*, https://en.wikipedia.org/wiki/Waveguide_%28optics%29 [Online].

[11] A. L. Gaeta, M. Lipson, T.J Kippenberg, "Photonic chip–based frequency combs," *Nature photonics 13*, 158-169, Feb. 2019. https://www.nature.com/articles/s41566-019-0358-x [Online].

[12] L. Cortes-Herrera, X. He, J. Cardenas, G.P. Agrawal, "Coupled-mode theory of the polarization dynamics inside a microring resonator with a uniaxial core," *Physical Review A*, vol. 103, 063517, Jun. 2021. https://labsites.rochester.edu/agrawal/wp-content/uploads/2021/06/PhysRevA.103.063517.pdf [Online].

[13] John M. Senior, *Optical Fiber Communications Principles and Practice*, 2009. https://shijuinpallotti.files.wordpress.com/2019/07/optical-fiber-communications-principles-and-pr.pdf [Online].

[14] W. Bogaerts, P. De Heyn, T. Van Vaerenbergh, K. De Vos, S. Kumar Selvaraja, T. Claes, P. Dumon, P. Bienstman, D. Van Thourhout, R. Baets, "Silicon microring resonators," *Laser Photonics 6*, no. 1, 47-73, 2012. https://www.photonics.intec.ugent.be/download/pub_3105.pdf [Online].

[15] StudySmarter, "Cavidad resonante," *StudySmarter*, https://www.studysmarter.es/resumenes/fisica/electromagnetismo/cavidad-resonante/ [Online].

[16] P. Liu, Q. Ji, J. Liu, J. Ge, M. Li, J. Guo, W. Jin, M. Gao, Y. Yu, A. Feshali, M. Paniccia, J. E. Bowers, K. J. Vahala "Near-visible integrated soliton microcombs with detectable repetition rates", *Nature Communications 16*, 4780, May 2025. https://doi.org/10.1038/s41467-025-60157-x [Online].

[17] ResearchGate contributors, "Schematic plot showing the free spectral range (FSR) and full width half max (FWHM) of a filter," *ResearchGate*, https://www.researchgate.net/figure/Schematic-plot-showing-the-free-spectral-range-FSR-and-full-width-half-max-FWHM-of-a_fig6_353655631 [Online].

[18] R. Paschotta, "Kerr Effect," *RP Photonics Encyclopedia*, https://www.rp-photonics.com/kerr_effect.html [Online].

[19] T. Herr, V. Brasch, J.D. Jost, C. Y. Wang, N. M. Kondratiev, M. L. Gorodetsky, T. J. Kippenberg, "Temporal solitons in optical microresonators," *Nature Photonics 8*, 145-152, Dec. 2013. https://www.nature.com/articles/nphoton.2013.343 [Online].

[20] Y.Qu, J. Wu, Y. Zhang, Y. Yang, L. Jia, H. El Dirani, S. Kerdiles, C. Sciancalepore, P. Demongodin, C. Grillet, C. Monat, B. Jia, D. J. Moss, "Integrated optical parametric amplifiers in silicon nitride waveguides incorporated with 2D graphene oxide films", *Light: Advanced Manufacturing 4*, no. 39, Dec. 2023. https://www.light-am.com/article/doi/10.37188/lam.2023.039 [Online].

[21] C. Bao, Y. Xuan, J. A. Jaramillo-Villegas, D. E. Leaird, M. Qi, A. M. Weiner, "Thermo-Optical Chaos and Direct Soliton Generation in Microresonators," *arXiv preprint*, Jan. 2017. https://arxiv.org/pdf/1701.03554 [Online].

[22] V. Brasch, M. Geiselmann, T. Herr, G. Lihachev, M. H. P. Pfeiffer, M. L. Gorodetsky, T. J. Kippenberg, "Photonic chip–based optical frequency comb using soliton Cherenkov radiation," *Science 351*, no. 6271, Dec. 2015. https://www.science.org/doi/10.1126/science.aad4811 [Online].

[23] T. J. Kippenberg, A. Gaeta, M. Lipson, M. L Gorodetsky, "Dissipative Kerr solitons in optical microresonators," *Science*, Jul. 2017. https://www.science.org/doi/10.1126/science.aan8083 [Online].

[24] Y. K. Chembo, N. Yu, "Modal expansion approach to optical-frequency-comb generation with monolithic whispering-gallery-mode resonators," *Physical Review A 82*, 033801, Sep. 2010. https://journals.aps.org/pra/abstract/10.1103/PhysRevA.82.033801 [Online].

[25] Y. K. Chembo, C. R. Menyuk, "Spatiotemporal Lugiato-Lefever formalism for Kerr-comb generation in whispering-gallery-mode resonators," *Physical Review A 87*, 053852, May 2013. https://journals.aps.org/pra/abstract/10.1103/PhysRevA.87.053852 [Online].

[26] C. Bao, J. A. Jaramillo-Villegas, Y. Xuan, D. E. Leaird, M. Qi, A. M. Weiner, "Observation of Fermi-Pasta-Ulam Recurrence Induced by Breather Solitons in an Optical Microresonator," *Physical Review Letters 117*, 163901, Oct. 2016. https://journals.aps.org/prl/abstract/10.1103/PhysRevLett.117.163901 [Online].

[27] M. Suh, K. J. Vahala, "Soliton microcomb range measurement," *Science 359*, 6378, Feb. 2018. https://www.science.org/doi/10.1126/science.aao1968 [Online].

[28] Yokogawa, “Optical Spectrum Analyzers,” *Test&Measurement,* https://tmi.yokogawa.com/us/solutions/products/optical-measuring-instruments/optical-spectrum-analyzers/#:~:text=An%20optical%20spectrum%20analyzer%20(OSA,wavelength%20in%20the%20horizontal%20scale. [Online].

[29] T. Domínguez Bucio, I. Skandalos, E. Sandell, M. Blasco, J. Faneca, V. Vitali, C. Lacava, P. Petropolous, F. Y. Gardes, “Silicon nitride integrated photonics: enabling versatile PICs for diverse applications,” *Proceedings of SPIE 13369*, Mar. 2025 https://www.spiedigitallibrary.org/conference-proceedings-of-spie/13369/1336906/Silicon-nitride-integrated-photonics--enabling-versatile-PICs-for-diverse/10.1117/12.3052665.short [Online].

[30] A. Yariv, “Coupled-mode theory for guided-wave optics,” *IEEE Journal of Quantum Electronics*, Sep. 1973. [Online]. Available: https://ieeexplore.ieee.org/stamp/stamp.jsp?tp=&arnumber=588673

[31] C. Liu et al., “Recent advances in silicon photonics: Devices and applications,” *Micromachines*, Dec. 2022. [Online]. Available: https://www.mdpi.com/2072-666X/13/12/2125

[32] X. Zhang, “Fano resonances in a multimode waveguide coupled to a high-Q silicon nitride ring resonator,” *Optics Express*, Apr. 2014. [Online]. Available: https://www.researchgate.net/publication/261069160_Fano_resonances_in_a_multimode_waveguide_coupled_to_a_high-Q_silicon_nitride_ring_resonator

[33] J. Chen et al., “Recent Advances in Optical Sensors,” *Sensors*, Dec. 2023. [Online]. Available: https://www.mdpi.com/1424-8220/23/24/9767

[34] D. Moss, “Bistability and Thermal Studies in High Index Doped Silica Integrated Ring Resonators,” *Preprints*, 2023. [Online]. Available: https://www.preprints.org/manuscript/202309.0780/v2